LBL-32418
UC-000

Lawrence Berkeley Laboratory
UNIVERSITY OF CALIFORNIA

EARTH SCIENCES DIVISION

Analysis of Flow Processes during TCE Infiltration in Heterogeneous Soils at the Savannah River Site, Aiken, South Carolina

K. Pruess

June 1992

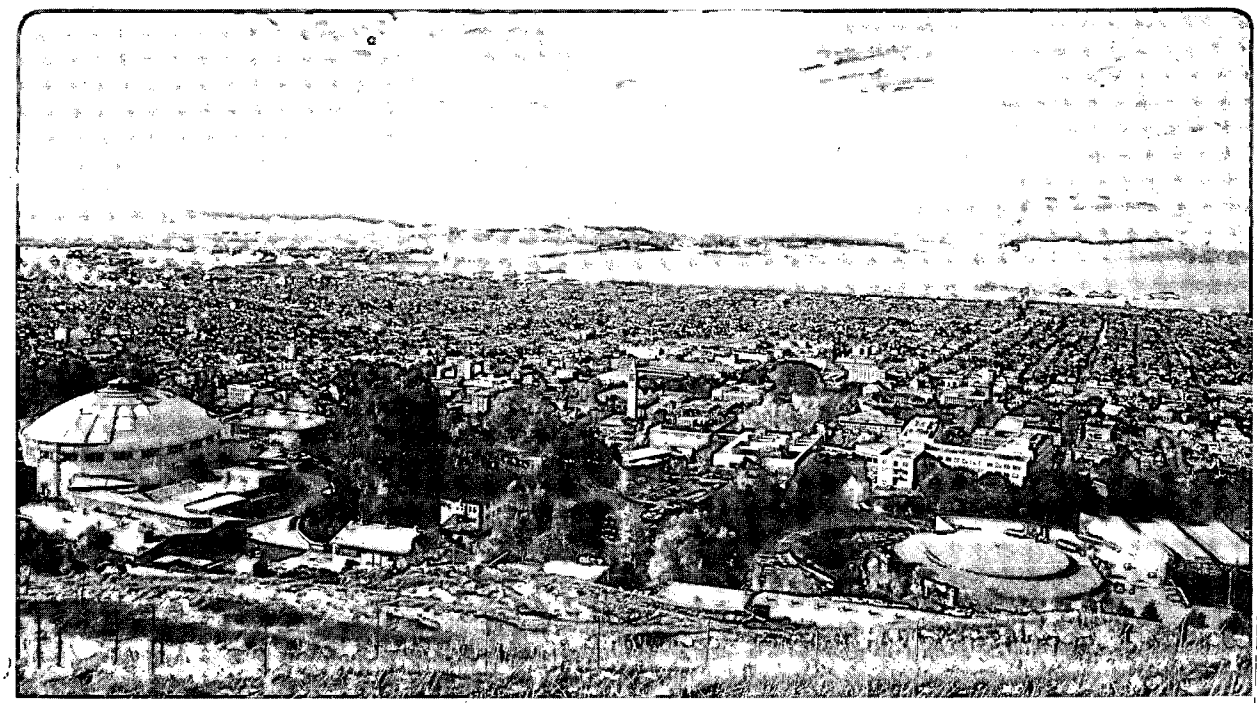

Prepared for the U.S. Department of Energy under Contract Number DE-AC03-76SF00098

DISCLAIMER

DISCLAIMER

LBL-32418

Analysis of Flow Processes during TCE Infiltration in Heterogeneous Soils at the Savannah River Site, Aiken, South Carolina

Karsten Pruess

Earth Sciences Division
Lawrence Berkeley Laboratory
University of California
Berkeley, California 94720

June 1992

This work was supported by the Assistant Secretary, Office of Environmental Restoration and Waste Management, Office of Technology Development, under U.S. Department of Energy Contract No. DE-AC03-76SF00098.

LBL-32418

Analysis of Flow Processes during TCE Infiltration in Heterogeneous Soils at the Savannah River Site, Aiken, South Carolina

Karsten Pruess

Earth Sciences Division, Lawrence Berkeley Laboratory
University of California, Berkeley, CA 94720

Introduction

Contamination of soils and groundwater from volatile organic compounds (VOCs), such as organic solvents and hydrocarbon fuels, is a problem at many industrial facilities. Key to successfully characterizing, containing, and eventually remediating the contamination is a thorough understanding, based on sound scientific principles, of the complex interplay of physical, chemical, and biological processes in geologic media, which affect the migration and distribution of the contaminants, and their response to remediation operations. A qualitative and quantitative understanding of contaminant behavior under natural conditions can provide valuable guidance for site characterization and monitoring. It can aid in evaluating the contamination that is likely to occur if no intervention is made (''no action'' scenario), and it provides useful information for the design and implementation of remedial actions. Sound engineering design of containment and remediation of contaminants must be based on mechanistic models that adequately describe the important contaminant migration processes; such models must be calibrated and validated through appropriate site data.

This report focusses on physical mechanisms that affect contaminant behavior under the conditions encountered at the Savannah River site (SRS). Although other contaminants are present at the site, for the purpose of this discussion we will restrict ourselves to the processes following a spill and infiltration of trichloroethylene (TCE), which is the main contaminant at the location of the Integrated Demonstration Project. We begin by briefly describing the main physical processes following release of TCE into the subsurface. Subsequently we will present simple engineering models that can help to evaluate contaminant migration processes in a semi-quantitative way. Finally, we will discuss results of detailed numerical simulations of TCE infiltration into a

heterogeneous medium consisting of sands and clays. These simulations attempt to shed light on the initial distribution of contaminants at the site prior to the start of remediation operations. We also point out limitations of present numerical modeling capabilities, and identify issues that require further research in order that a realistic description of contaminant behavior in the subsurface may be achieved.

Contaminant Behavior under Natural Conditions

The infiltration of TCE into the subsurface gives rise to a number of coupled multi-phase partitioning and flow processes in a three-phase system consisting of an aqueous phase, a gas phase, and a non-aqueous phase liquid (NAPL). Table 1 lists some of the important thermophysical properties that determine contaminant behavior.

Table 1. Selected thermophysical properties of water, air, and TCE at ambient conditions of 20°C temperature, 1 bar pressure (as used in STMVOC code)

Component	Water	Air	TCE
density (kg/m^3)	998.2	1.19	1462
viscosity (Pa.s)	1.00×10^{-3}	1.66×10^{-5}	$.59 \times 10^{-3}$
vapor pressure (kPa)	2.337	-	7.196
effective density in phases (kg/m^3)			
aqueous (*)	997.2	.0145	1.099
gas (*)	.017	1.07	.388
NAPL	-	.003	1462

(*) assuming that all three components are present

The density of TCE being approximately 1462 kg/m^3 at ambient conditions, as compared to 1.2 kg/m^3 for soil gas (humid air) and 998 kg/m^3 for water, a plume of NAPL will migrate downwards under the combined action of gravity, viscous, and capillary forces. Because of heterogeneities on different scales, such as clay lenses and depositional layers that differ in permeability, porosity, and capillary behavior, the NAPL will not flow straight downward in a piston-like displacement, but will instead be dispersed to varying degree both vertically and horizontally. Partial ponding may occur when the plume encounters regions of low permeability or adverse wettability, such as clays. The

presence of aqueous and gas phases in the pore space will interfere with the NAPL migration (relative permeability effects). It will also impact on the NAPL by way of phase partitioning processes, namely, dissolution in the aqueous phase, and evaporation into the gas phase. At ambient conditions of T = 20°C, P = 1 bar, the partial density of TCE in a saturated aqueous solution is 1.10 kg/m^3, while the density of saturated TCE vapor is .39 kg/m^3. Thus, the amount of TCE in 1 m^3 of free product, 1462 kg/m^3, is equal to the TCE content in 1330 m^3 of saturated aqueous solution, and 3768 m^3 of vapor-saturated gas. The TCE can also sorb on solid phases, such as organic carbon and soil minerals. This sorption may be partially or completely reversible, and it may occur instantaneously (equilibrium sorption) or be controlled by kinetic rates. Portions of the NAPL plume may also be immobilized in the pore space by capillary force.

The downward advancement of a TCE plume is an intrinsically unstable process, because higher-density fluid (TCE) is present above fluids of lower density (water, soil gas). Interacting with ever present soil heterogeneities on different scales, the gravitational instability may give rise to a highly dispersed displacement front (fingering). Because TCE is denser than water, a plume of TCE will continue to sink downward below the water table, and will tend to migrate to deep and poorly accessible regions.

The presence of TCE vapors considerably increases the density of soil gas. At ambient conditions of T = 20°C, P = 1 bar, the density of (humid) air is 1.18 kg/m^3, while the density of air saturated with TCE vapor is 1.48 kg/m^3. This density contrast provides a negative (downward) buoyancy force which can induce large-scale gas phase convection with associated spreading of the contaminant (Falta et al., 1989). Additional mechanisms for contaminant spreading through gas phase processes include molecular diffusion, and barometric pumping.

Gravity-driven Flow of a NAPL Plume

Neglecting effects from capillary and pressure forces, the flux in a NAPL plume that is falling freely under gravity in the vadose zone can be estimated from a multiphase version of Darcy's law as

$$F_n = k \frac{k_{rn}}{\mu_n} \rho_n^2 g \qquad (1)$$

Here F_n is mass flux in kg/s m^2, k and k_{rn} are absolute and relative permeability, respectively, ρ_n is NAPL density, μ_n is NAPL viscosity, and g is the acceleration of gravity. In writing Equation (1) we have neglected the small density of soil gas relative to liquid NAPL. Inserting values of ρ_n = 1462 kg/m^3 and $\mu_n = 0.59 \times 10^{-3}$ Pa.s appropriate for

TCE, Equation (1) gives

$$F_n = k \cdot k_{rn} \times 3.554 \times 10^{10} \qquad (kg/s) \tag{2}$$

If NAPL is spilled at a mass rate Q (kg/s), the horizontal cross sectional area A_Q to which the plume will spread can be estimated from

$$Q = A_Q \cdot F_n \tag{3}$$

Substituting from Equation (1) we have

$$A_Q = \frac{\mu_n Q}{k\, k_{rn}\, \rho_n^2 g} \tag{4}$$

Inserting parameters appropriate for TCE, this gives

$$A_Q = \frac{1.81 \times 10^{-11}}{k\, k_{rn}} Q \qquad (m^2) \tag{5}$$

A similar discussion can be made for gravity-driven migration of NAPL below the water table. In this case the effective body force on the NAPL is $(\rho_n - \rho_w) * g$, so that the flux can be estimated as

$$F_n = k \frac{k_{rn}}{\mu_n} \rho_n (\rho_n - \rho_w) g \tag{6}$$

which is a factor $(\rho_n - \rho_w)/\rho_n = (1462-998)/1462 = .32$ smaller than the corresponding expression Equation (1) for the vadose zone.

Suppose that a TCE plume advances downward by building to a saturation $S_{TCE} = 1 - S_{wr}$. The rate at which the TCE plume advances can then be estimated from

$$\phi(1 - S_{wr})\rho_n u_n = F_n \tag{7}$$

Here u_n is the actual (pore) velocity of TCE advancement. For plume propagation in the vadose zone we have, from Equations (1) and (7)

$$u_n = k\, k_{rn} \frac{\rho_n g}{\phi(1 - S_{wr})\mu_n} \tag{8}$$

NAPL Mobilization by Buoyant Gas Flow

Buoyant gas flow due to the presence of a volatile organic compound (VOC) such as TCE was discussed by Falta et al. (1989). The Darcy velocity (volumetric flux) of downward gas flow can be estimated in analogy to Equations (1) and (6) as

$$v_{gas} = k\frac{k_{rg}}{\mu_g}(\rho_g - \rho_{air})g \tag{9}$$

Here ρ_g is the density of gas containing a mixture of (moist) air and VOC vapor, while ρ_{air} is the density of ambient soil gas. The VOC mass flux associated with the volumetric flux of Equation (9) is obtained by multiplying with the partial density ρ_{gn} of contaminant vapors in the gas phase. In the presence of free NAPL phase the appropriate density is the saturated vapor density ρ_{gn}^0 which from the ideal gas law can be estimated as

$$\rho_{gn}^0 = \frac{P^0 M}{RT} \tag{10}$$

where P^0 is the saturated vapor pressure of the VOC, M is the molecular weight, R the universal gas constant, and T the absolute temperature. Adopting ideal-gas approximations also for the densities of air and air/vapor mixtures, Equations (9) and (10) combine to yield a VOC vapor flux

$$E = k\,k_{rg}\frac{g}{\mu_g}\left[\frac{P^0}{RT}\right]^2 M(M - M_{air}) \tag{11}$$

We have denoted the buoyant downward mass flux of VOC vapors by E, because, under presumed conditions of local phase equilibrium, it must equal the evaporation rate of free NAPL phase per unit horizontal cross sectional area. At T = 20°C, saturated vapor pressure of TCE is 7.2 kPa, and air viscosity is 1.66×10^{-5} Pa.s, so that from Equation (11) we have

$$E = k\,k_{rg} \times 6.94 \times 10^4 \ (kg/m^2{\cdot}s) \tag{12}$$

Assuming that NAPL is present at irreducible saturation S_{nr}, the thickness of NAPL layer removed per unit time from buoyant gas flow, $\dot{d}_g$, can be estimated from

$$E = \phi S_{nr} \rho_n \dot{d}_g \tag{13}$$

Inserting typical parameters of $k\,k_{rg} = 1. \times 10^{-11}$ m^2, $\phi = .4$, $S_{nr} = .05$, $\rho_n = 1462$ kg/m^3, we have $\dot{d}_g = 2.38 \times 10^{-8}$ m/s = .75 m/yr, which represents a significant amount of contaminant removal.

NAPL Leaching by Water

An analysis similar to the above can be made for removal of free NAPL phase by means of leaching from infiltrating water. An infiltrating volumetric water flux v_w will dissolve NAPL at a rate of

$$D = v_w \rho_{wn} \tag{14}$$

where ρ_{wn} is the partial density of NAPL in saturated aqueous solution. Again assuming that NAPL is present at irreducible saturation S_{nr}, the thickness of NAPL layer removed per unit time from dissolution in infiltrating groundwater, $\dot{d}_w$, can be estimated from

$$D = \phi S_{nr} \rho_n \dot{d}_w \tag{15}$$

It is of interest to compare the rates of NAPL removal by buoyant gas flow and dissolution in infiltrating ground water. For parameters applicable to TCE we have, from Equations (12) and (14)

$$\frac{E}{D} = \frac{k\, k_{rg}}{v_w} \times \frac{6.94 \times 10^4}{1.1} = 63.09 \times 10^3 \frac{k\, k_{rg}}{v_w} \tag{16}$$

For a hypothetical water infiltration rate of 1 m/yr, this ratio becomes

$$\left[\frac{E}{D}\right]_{v_w = 1 m/yr} = 1.991 \times 10^{12}\, k\, k_{rg} \tag{17}$$

so that evaporation of NAPL into gas phase flowing under buoyancy would equal dissolution into infiltrating groundwater at an effective gas permeability of $1/1.991 \times 10^{12}$ m^2 = $.55 \times 10^{-12}$ m^2, or .55 darcy. For higher permeability evaporation would dominate, while for lower permeability dissolution would be a more important mechanism for NAPL removal.

Gas Diffusion

The spreading of VOC vapors in the gas phase by molecular diffusion has been discussed by Falta et al. (1989). It is described by a diffusion equation

$$\frac{\partial X_g^c}{\partial t} = D_{g,eff}\, \Delta X_g^c \tag{18}$$

where X_g^c is the mass fraction of VOC vapor in the gas phase, and the effective gas diffusivity is given by

$$D_{g,eff} = \frac{\tau}{R_g} D_g \tag{19}$$

Here, τ is a tortuosity factor, typically of order 0.5, and R_g is the gas phase retardation factor, which accounts for phase partitioning of VOC vapors into liquid and solid phases through dissolution and sorption, respectively. The retardation factor is

$$R_g = 1 + \frac{S_w}{S_g H} + \frac{\rho_g K_D}{\phi S_g H} \tag{20}$$

Here

$$H = \frac{C_g}{C_w} \tag{21}$$

is Henry's constant, which is the ratio of effective densities (concentrations) $C_g = \rho_g * X_g^c$ and $C_w = \rho_w * X_w^c$ of the contaminant in gas and water phases, respectively.

$$K_D = \frac{X_s^c}{C_w} = K_{oc} f_{oc} \tag{22}$$

is the distribution coefficient for the VOC chemical between solid and aqueous phases, given by the ratio of mass fraction of adsorbed VOC in the solid phase, X_s^c, to effective density of VOC dissolved in the aqueous phase. This is usually assumed to be proportional to fraction of organic carbon, f_{oc}, in the soil, the proportionality factor K_{oc} being referred to as the organic carbon partition coefficient.

For TCE, we have H = .388 / 1.099 = .353. Assuming that adsorption is insignificant at Savannah River (Eddy et al., 1991), the gas phase retardation factor for a typical irreducible water saturation of $S_{wr} = .15$ is approximately 1.5. For a typical ''free'' gas diffusivity of 10^{-5} m^2/s, the effective gas diffusivity from Equation (19) then becomes 3.3×10^{-6} m^2/s. To put this number in perspective it may be compared with a typical thermal diffusivity for heat conduction in soils, which is $D_{th} = K/\rho * c = 1.5/2500 * 1000 = 0.6 \times 10^{-6}$ m^2/s. The distance to which diffusive spreading reaches can be estimated as

$$x = \sqrt{Dt} \tag{23}$$

Thus, diffusive spreading of TCE in the gas phase is somewhat more rapid (by a factor $\sqrt{3.3/0.6} = 2.3$) than conductive heat transfer in soils, but it is a relatively slow process. Based on the effective gas phase diffusivity of 3.3×10^{-6} m^2/s for TCE estimated above, diffusive penetration distances are .53 m in 1 day, 10.2 m in 1 year, and 32.3 m in 10 years.

Barometric Pumping

VOC vapors may be removed from the subsurface as a result of atmospheric pressure variations, a process that we shall refer to as ''barometric pumping.'' Atmospheric pressure is subject to fluctuations with a dominant cycle period of 24 hours. As atmospheric pressure rises, the column of soil gas above the water table is compressed, and ''clean'' atmospheric air enters the subsurface, where it may acquire some VOC contamination through processes such as mixing with already contaminated soil gas, evaporation

of resident NAPL, or diffusion of VOC vapors down concentration gradients. When atmospheric pressure subsequently decreases, the soil gas column expands, discharging a certain amount of contaminant to the atmosphere.

The quantitative aspects of this process may be estimated in analogy to the problem of moisture removal from the vadose zone by barometric pumping (Tsang and Pruess, 1989). From the ideal gas law, decrease of atmospheric pressure from $P \rightarrow P - \Delta P$ will result in an increase in the height of the soil gas column from $H \rightarrow H + \Delta H$ such that

$$\frac{\Delta P}{P} = \frac{\Delta H}{H} \tag{24}$$

Per unit surface area, the amount of VOC vapor removed in one full pressure cycle will be

$$M_{VOC} = \Delta H \, \phi \, S_g \, \rho_{gn} = H \left[\frac{\Delta P}{P} \right] \phi \, S_g \rho_{gn} \tag{25}$$

For an order-of-magnitude estimate, we use $\Delta P/P = .005$ (Tsang and Pruess, 1989), and $H = 40$ m, $\phi = .4$, $S_g = .8$, to obtain a removal of VOC vapors of $.064 * \rho_{gn}$ kg/m^2 per pressure cycle (one day). Making the extreme assumption that VOC vapor in soil gas beneath the land surface is at saturated density of .39 kg/m^3, this translates into a removal of 788 kg/m^2 per year, a very large amount. Realistically, however, VOC vapor concentration will likely be much less than saturated near the ground surface, so that contaminant removal rates from atmospheric pumping will be considerably less. For the parameters assumed above, the thickness of soil layer beneath the ground surface that is directly affected by barometric pumping is only $\Delta H = .005 * H = 0.2$ m. After removal of free NAPL phase from this zone immediately beneath the ground surface, VOC vapors can be supplied to the atmospheric pumping process only by diffusion from below (as convective transport is downward). The long-term impact of atmospheric pumping thus seems to be to effectively shift the atmosperic "zero VOC concentration" boundary downward by a small distance of order $\Delta H = 0.2$ m, which is not expected to have a significant effect on contaminant migration.

Numerical Simulation of TCE Infiltration

Some of the important processes affecting contaminant migration and dispersal may operate on relatively small spatial scales (< 1 m), which may not be resolvable with the kind of spatial discretization that would normally be employed in engineering models of a site. For example, observations at the Savannah River site indicate that TCE contamination is highly spatially variable, and tends to be localized near the top of clay-rich

zones (Eddy et al., 1991). The strong heterogeneity of contaminant distribution has important implications for the feasibility and success of remediation operations. We need to understand why the contaminant is distributed in the observed manner, and what the driving forces and conditions are that have generated this kind of distribution. Only if we identify the processes leading to the observed contaminant distribution can we hope to be able to perform a reliable evaluation of remediation schemes, and to develop an understanding of what the processes can and cannot accomplish in a given time frame. Such process understanding is also essential for a transfer of the experience gained at Savannah River to other sites.

In this section we report on the current status of our efforts to use multiphase numerical simulation as a tool for developing a better understanding of the role of formation heterogeneity in contaminant transport. In order to be able to identify the manner in which the different multiphase flow and partitioning processes interact with formation heterogeneity we have simulated idealized "generic" models, which were designed to capture important features of the Savannah River site, such as layering of highly permeable sands with clays of variable horizontal extent. Rather than modeling the full complement of multiphase processes in a complex heterogeneous setting, we introduce process and formation complexity in a step-wise fashion, to be able to discern the important controls on contaminant behavior. For example, we examine in considerable detail the interaction of a descending TCE plume with clay lenses and clay layers of different spatial extent, both in the vadose zone and beneath the water table. It is hoped that the insight gained from such detailed studies will eventually support a scale-up to "effective" process description on a larger scale.

Numerical modeling of TCE infiltration is subject to space discretization effects (numerical dispersion), which can be particularly severe because of the gravitationally unstable nature of the process (Pruess, 1991). These effects can give rise to spurious (unphysical) flows, which may depend strongly on size and orientation of the numerical grid used. We have performed a grid orientation study to specifically address these isssues (below).

TOUGH2 and STMVOC Codes

The simulations reported here were carried out with the TOUGH2 and STMVOC simulators, which are closely related members of the TOUGH/MULKOM family of multiphase simulation codes, developed at Lawrence Berkeley Laboratory. TOUGH2, a successor to TOUGH, is a general-purpose simulator for nonisothermal flows of multiphase,

multicomponent fluids (Pruess, 1987, 1991). STMVOC, a descendent of TOUGH, features the same general architecture and solution methodology (Falta and Pruess, 1991; Falta et al., 1992a). It is a specialized code for nonisothermal flow of three-phase three-component mixtures of water, air (a pseudo-component) and a volatile organic compound (VOC). STMVOC describes all of the multiphase processes discussed above, including full phase partitioning of the VOC between NAPL, gas, aqueous, and solid phases, VOC migration by convection in all of the three phases, and VOC diffusion in the gas phase. It has full capabilities to describe strongly heat-driven processes, such as steam drive of volatile contaminants. However, in the present study STMVOC has been used only for processes at ambient temperature of 20°C. The code has been validated by comparison with laboratory experiments (Falta et al., 1992b).

Model System

The model system is loosely patterned after the conditions at the site of the SRS Integrated Demonstration Project (see Figures 1 and 2). The main contaminant source being a process sewer line of considerable horizontal length, we model a 2-D vertical (X-Z) section perpendicular to the sewer line. Constant gas pressure conditions are maintained at the ground surface, and constant gas and aqueous phase pressures are maintained at the distant lateral boundaries. The water table is placed at a depth of approximately 130 ft (Eddy et al., 1991). Total vertical extent of the system modeled is 160 ft, at which depth boundary conditions of "no flow" or "constant pressure" are imposed.

For the simulations reported below STMVOC was run in isothermal mode, with the entire flow system held at a temperature of 20°C by means of assignment of a very large heat capacity to the porous medium.

Some of the parameters that have an important impact on the behavior of the three-phase water-air-NAPL system are poorly known. This is especially true for the "characteristic curves" (relative permeability and capillary pressure curves). For relative permeabilities we have adopted a functional relationship developed by Stone (1970) that is widely used in petroleum reservoir engineering. This relationship had to be slightly modified to deal with subtle issues of phase behavior near irreducible saturations. The equations for water, gas, and NAPL phase relative permeability used here are:

$$k_{rw} = \left[\frac{S_w - S_{wr}}{1 - S_{wr}}\right]^n \tag{26}$$

$$k_{rg} = \left[\frac{S_g - S_{gr}}{1 - S_{wr}}\right]^n \tag{27}$$

$$k_{rn} = \left[\frac{1-S_g-S_w-S_{nr}}{1-S_g-S_{wr}-S_{nr}}\right]\left[\frac{1-S_{wr}-S_{nr}}{1-S_w-S_{nr}}\right]\left\{\frac{(1-S_g-S_{wr}-S_{nr})(1-S_w)}{(1-S_{wr})}\right\}^n \qquad (28)$$

The modification made concerns the term in the curly brackets for k_{rn}, where we have replaced Stone's expression $(1-S_g-S_{wr})$ by $(1-S_g-S_{wr}-S_{nr})$, to avoid the unphysical possibility of obtaining large k_{rn} near S_{nr} when S_g is near $1-S_{wr}-S_{nr}$.

For capillary pressures we used the three-phase relationships given by Parker et al. (1987); however, capillary pressure between gas and NAPL phases was neglected. The capillary pressure between the aqueous phase and the non-wetting gas and NAPL phases is

$$P_{cgw} = -\frac{\rho_w g}{\alpha_{nw}}\left[\left(\frac{1-S_m}{S_w-S_m}\right)^{\frac{n}{n-1}}-1\right]^{1/n} \qquad (29)$$

A summary of problem specifications intended to be representative of conditions at the site of the Savannah River integrated demonstration project is given in Table 2. Capillary pressures for different hydrogeologic units were scaled inversely to the square root of absolute permeability.

Table 2. Formation Properties for 2-D Vertical Section Problem

		Sands	Clayey Sands	Clays
permeability (m^2)	k	10^{-11}	10^{-12}	10^{-15}
porosity	ϕ	.35	.35	.50
relative permeabilities (Equations 26-28)				
irreducible water saturation	S_{wr}	.15	.60	.60
irreducible gas saturation	S_{gr}	.001	.001	.001
irreducible NAPL saturation	S_{nr}	.05	.05	.05
exponent	n	3	3	3
capillary pressures (Equation 29)				
strength parameter	α_{nw}	5.0	1.58	.05
limiting saturation	S_m	0.0	0.0	0.0
exponent	n	1.84	1.84	1.84

The flow domain is a 1 m thick vertical section, with dimensions of 160 ft in the vertical,

1000 ft horizontally. For numerical simulation it is discretized into 24 rows and 15 columns of varying spacing (Figure 3). Finer vertical discretization was employed at the elevations at which clays are encountered at the site, to be able to better resolve flow processes associated with those clays. Horizontal discretization is finest near the assumed symmetry line (left hand side) where TCE release is taking place. An expanded view of a part of the calculational mesh is shown in Figure 4, which also indicates the assignment of domains with different hydrologic properties. The domains labeled "325CL" and "300CL," respectively, correspond to the 325 ft and 300 ft clays encountered at the site (Figure 1), and are assigned clay properties as given in Table 2. The domain "TANCL" represents a clayey sand corresponding to the "tan clay" at the site. It should be emphasized that in its present form the assignment of these units and their hydrologic properties is rather schematic. They are meant to represent the hydrogeologic features of the site in a generic way, so that important process aspects may be explored. The description of hydrogeologic units and the specification of their properties needs to be refined in the future, so that natural conditions and remediation response may be modeled in more realistic detail.

Prior to startup of TCE infiltration, the system was run to gravity-capillary equilibrium. Water saturation in the vadose zone was assumed to be at irreducible levels. For the initial set of runs no water recharge from the surface was taken into account. The contaminant is assumed to be pure TCE with thermophysical properties as given for problem 3 in the STMVOC User's Guide (Falta and Pruess, 1991). Release of contaminant is modeled by injecting TCE into the uppermost grid block at the left hand side of the model, at a rate of 89.68×10^{-6} kg/s, which is equivalent to 1 barrel per 30-day month. Because of symmetry we only model half of the domain, so that the spill rate amounts to 2 barrels of TCE per month per meter of sewer line.

Infiltration into Clayey Sands

We have modeled TCE infiltration over a time period of 30 years. For the following discussion of the behavior of the NAPL plume refer to Figures 5 and 6, which show NAPL saturation distributions after 3 years of infiltration in a large-scale and a close-up view, respectively.

In response to TCE release, NAPL saturation in the injection grid block builds up until the residual NAPL saturation of 5% is exceeded, at which point the NAPL becomes mobile and begins to flow downward under gravity. Eventually the descending NAPL plume encounters a clay lense (the "325CL" domain, Figure 4), which because of its low absolute and relative permeability acts as an obstacle to downflow of NAPL.

Ponding with buildup of NAPL saturation takes place, which is accompanied by modest pressure increase. This causes most of the NAPL to flow laterally, but a small amount of NAPL is slowly invading the clay zone itself, and ultimately passes right through it. The NAPL flowing laterally to circumvent the clay lense resumes its predominant downward flow after it reaches a break in the clay lense, and subsequently ponds again as it encounters the more extensive clay zone at 60 ft depth (the 300 ft clay). The growth of the ponded zone slows with time, as an increasing proportion of the infiltrating TCE penetrates into the clay. The extent of the ponded zone has almost stabilized after 10 years (compare Figures 7–9), eventually reaching an area of 38.1 m^2. From Equation (5) the ponded area may be estimated as $A_Q = 2.52/k_{rn}\ m^2$, which is consistent with the simulation results, but also indicates that because of the strong dependence of A_Q on the a priori unknown k_{rn}, Equation (5) is of limited utility in that it can only provide a very conservative lower bound. It is evident that a considerably broadened plume descends below the clay zone. After 30 years the plume has penetrated all the way into the water table, and NAPL saturation is beginning to build up at the bottom of the flow system, which was assumed impermeable in this simulation (see Figure 9).

In addition to a free-phase NAPL plume, a plume of TCE vapors develops in the gas phase (Figures 10–14). This plume spreads much more quickly to a large volume, because of gas phase convection driven by the negative buoyancy of vapor-ladden soil gas. From the shape of the concentration contours one can clearly see how the downward convection is diverted sideways as the lower permeability of the "TANCL" domain is encountered at a depth of 90 ft. The regions enclosed by the 0.3 kg/m^3 concentration contour correspond closely to the extent of the NAPL plume, as concentrations approaching the saturated value of 0.388 kg/m^3 can only be maintained in immediate proximity to free NAPL. Note also that, wherever TCE vapor is present, a TCE concentration in equilibrium with the gas phase concentrations is maintained in the aqueous phase. The amount of TCE dissolved per unit volume of aqueous phase is a factor 2.83 larger than what is present in the gas phase.

Diffusive transport of TCE vapors in the gas phase was neglected in the present calculation. As was discussed here diffusion will yield a migration distance of order 100 ft over 10 years, adding further spreading of the TCE vapor plume which is not insignificant, but is considerably smaller than the distance covered by advective transport. The advective migration of TCE vapors is probably overestimated in the simulation presented here, because of the rather small extent of clay zones in the model. The presence of more extensive clay layers with only limited breaks at Savannah River would tend to reduce gas convection effects.

Another simulation was run in which TCE infiltration was stopped after 10 years, and the system was left alone to examine the redistribution of contaminant that would occur under natural "no action" conditions. The NAPL plume after 10 years of infiltration followed by 20 years of no infiltration is shown in Figure 15, which should be compared to Figure 7 for the plume at 10 years. It is seen that the NAPL plume has continued to disperse outward and downward, while highest NAPL saturations have been reduced. There is a rather limited region above the clay lense where the NAPL has been removed by persistent evaporation into the descending gas stream. This simulation was continued to 100 years total time (results not shown), after which time NAPL was completely swept out of the region above the clay lense, with very significant NAPL saturations remaining in the clay lense itself (approximately S_n = 12%). A similar pattern of behavior was seen at the more extensive clay layer. This can be understood by noting that gas convection is confined to the highly permeable sands. Thus, although penetration of NAPL into the clays is inhibited by low absolute and relative permeability, NAPL that will get into the clays is little affected by gas phase redistribution processes.

A brief exploration of flow system behavior in the presence of water infiltration from precipitation was also made. Applying a recharge rate of 15 inch/year (Colven et al., 1987), the system was first run to steady state. This resulted in a modest increase in water saturations beyond irreducible levels in the highly permeable sands (from 15% to approximately 19%), while the clays became almost completely water-saturated (S_w > 98%). Steady water saturations for the case with recharge are shown in Figure 16. The attainment of nearly full water saturation by the clays can be understood by noting that the permeability of the clay units of 10^{-15} m^2 corresponds to a hydraulic conductivity of approximately 10^{-8} m/s, or .32 m/yr, which is slightly less than the applied recharge rate. Figure 16 shows that there is some increase of water saturation above the clays; part of the infiltrating flux is being diverted around the clay zones. After a steady state with 15 inch/ year of recharge was reached, TCE was injected at the same rate as in the previous set of simulations without water infiltration. The NAPL plume after 10 years is shown in Figure 17; it looks very different from the previous case of no water infiltration (Figure 7). The NAPL again ponds atop the clays, but due to their nearly complete water saturation the clays now act as nearly impermeable barriers to the NAPL, and very little NAPL penetration into the clays themselves takes place. Virtually all of the injected TCE is being diverted laterally around the clays. However, in the aqueous phase in the clay regions, TCE is present at close to saturated concentrations.

Grid Orientation Effects

In simulations of oil recovery operations involving two- or three-phase flow it has been noticed for a long time that predicted results can be sensitive to the orientation of the computational grid used. Mobilization of highly viscous oil by less viscous water or steam is an ''unfavorable mobility ratio'' displacement, which is subject to a hydrodynamic instability (viscous fingering). The finite space discretization used in finite difference or finite element numerical simulations generates a purely numerical (as opposed to physical) dispersion with associated spurious flows. Numerical dispersion in general will be anisotropic and tends to be strongest in the directions of the lines of the numerical grid, and weakest in the directions running diagonally to the grid. The ''grid orientation effect'' (spurious dependence of simulated results on the orientation of the numerical grid) arises from an interplay between hydrodynamic instability and anisotropic numerical diffusion (Brand et al., 1991).

In the context of oil recovery simulations, grid orientation effects have been discussed for horizontal flows, with particular focus on steam flooding (Todd et al., 1972; Coats et al., 1974; Coats, 1982; Coats and Ramesh, 1984). The customary approach has been to consider a five-spot production-injection arrangement, and to compare simulations with ''parallel'' and ''diagonal'' grids (Figure 18). It has been shown that grid orientation effects can be substantially reduced or eliminated by means of higher-order differencing schemes, which maintain a higher degree of rotational invariance. This results in a more nearly isotropic numerical dispersion, so that hydrodynamic instabilities will not be amplified from grid effects. Figure 19 depicts the standard ''5-point'' approximation, in which a grid block P interacts with the four neighbors with which it shares a common interface (solid flow lines). The ''9-point'' approximation additionally incorporates flow in the diagonal directions (dashed flow lines), which essentially eliminates grid orientation effects in the simulation of steam floods (Yanosik and McCracken, 1979; Coats and Ramesh, 1982; Pruess and Bodvarsson, 1983).

At a temperature of 20°C, the viscosity of TCE (0.59×10^{-3} Pa.s) is larger than the viscosity of air (1.66×10^{-5} Pa.s), but smaller than the viscosity of water (1.00×10^{-3} Pa.s). Thus displacement of air by TCE has a favorable mobility ratio, while displacement of water has an unfavorable mobility ratio, so that invasion of TCE into an aquifer would be subject to a viscous instability which, however, would not be very strong as the viscosities of TCE and water differ by less than a factor 2.

There is another kind of hydrodynamic instability which is of much more significance and concern with TCE, namely, the gravitational instability of a denser fluid (TCE) invading regions with less dense fluids (air, water) from above. This kind of

instability may lead to strong grid orientation effects in vertical section models. Such effects have been recently studied for the problem of cold water injection into depleted vapor zones in vapor-dominated geothermal reservoirs (Pruess, 1991). Issues of gravitational instability and the associated potential for grid orientation effects in the release of TCE into the vadose zone are entirely analogous to the geothermal injection problem. In order to evaluate these effects we have performed a simulation study that closely parallels the geothermal injection study.

Using the "EOS8" three-phase module of TOUGH2, we have simulated the migration of TCE plumes in vertical section models that employ parallel and diagonal grids, respectively (Figure 20). The grids shown in Figure 20 are meant to illustrate the concept; in the actual simulations we use a 12 × 12 parallel grid of 5m * 5m blocks, and a diagonal grid with 7.5 m long diagonal (5.303 m side length). The flow system is 1 m thick and the vertical and horizontal dimensions are 60 m each. The water table is at a depth of 37.5 m; constant pressure conditions are maintained at the right boundary, with all other boundaries being "no flow." TCE is injected in the left uppermost grid block at a rate of 89.68×10^{-6} kg/s, corresponding to 1 barrel per 30-day month. Simulations were performed for a ten-year period, using parallel and diagonal grids, and 5-point and 9-point differencing schemes. Results for TCE plumes after 10 years are shown in Figure 21, where shading indicates the presence of NAPL saturations of 1% or larger. Comparison of the 5-point results for parallel and diagonal grids shows that grid orientation effects are very large. The parallel grid produces a narrow TCE plume that slumps downward, and then spreads along the impermeable bottom of the flow system. In contrast, the diagonal grid gives considerable lateral spreading of the plume. A comparison of the 9-point results for both grids shows that grid orientation effects have been essentially completely eliminated.

It is to be emphasized that absence of grid orientation effects does not necessarily mean that physically realistic results have been obtained. It simply means that the anisotropy of numerical dispersion has been reduced in such a way that it will not amplify a hydrodynamic instability which is present in the flow system. Physically realistic modeling of the migration of a NAPL plume under conditions of a gravitationally induced hydrodynamic instability requires proper description of all physical mechanisms that will affect plume dispersion in a heterogeneous medium. In the absence of heterogeneity, the downward slumping predicted by the parallel 5-point grid is actually correct, because this differencing scheme produces numerical dispersion only in the vertical direction (Pruess, 1991). A lateral (transverse) spreading of the plume can arise from formation heterogeneity, such as presence of clay lenses and layers, as was demonstrated in the numerical

simulations discussed above. Although diagonal grids and higher-order differencing methods produce more nearly isotropic dispersion effects, there is no reason to expect the lateral dispersion in these differencing schemes to adequately approximate true physical dispersion effects in a heterogeneous medium. We believe that the 5-point parallel differencing scheme is acceptable when heterogeneities are modeled in explicit detail. The 5-point diagonal as well as parallel and diagonal 9-point schemes introduce a lateral numerical dispersion that in detailed models with explicit representation of heterogeneity would arise from flow diversion due to the heterogeneities. A physically realistic representation of the dispersive effects of heterogeneity in continuum-based numerical models of multiphase flow has yet to be developed.

Concluding Remarks

We have presented engineering estimates as well as numerical simulations for the multiphase processes that arise from TCE release in the vadose zone. Although the basic physico-chemical processes of flow and phase partitioning are simple and well understood, their analysis is complicated by numerous coupled effects and by the ever-present and always imperfectly known heterogeneity of geologic media. Our simulations help to explain the preferential association of TCE contamination with clays that was observed at the Savannah River site (Eddy et al., 1991). Buoyancy flow in the gas phase was found to have a potential for spreading contamination from localized sources over large areas.

Although a large amount of data is available for the site, some of the most important parameters affecting TCE behavior in the vadose zone, such as three-phase relative permeabilities and capillary pressures, are poorly known. Presently available simulation techniques can cope with the highly nonlinear multiphase processes affecting TCE migration in the subsurface. Further research is needed to develop a better understanding of the behavior of multiphase fluid mixtures in heterogeneous systems.

In future projects dealing with subsurface contamination, it would seem beneficial to integrate simulation-based performance assessment modeling as early and closely as possible with the site characterization, monitoring, and remediation activities.

Acknowledgement

This work was supported through the Office of Technology Development, U.S. Department of Energy, under contract DE-AC03-76SF00098. The author appreciates the collaboration of managers and technical staff of the Westinghouse Savannah River

Company, and acknowledges helpful technical discussions with Dwayne Chesnut, Lawrence Livermore National Laboratory. Thanks are due to Y. Tsang for a critical review of the manuscript.

References

Brand, C. W., Heinemann, J. E. and Aziz, K., The Grid Orientation Effect in Reservoir Simulation, paper SPE-21228, presented at Society of Petroleum Engineers Eleventh Symposium on Reservoir Simulation, Anaheim, CA, February 1991.

Coats, K. H., Reservoir Simulation: State of the Art, *J. Pet. Tech.,* 1633-1642, August 1982.

Coats, K. H., George, W. D., Chu, C. and Marcum, B. E., Three-Dimensional Simulation of Steamflooding, *Soc. Pet. Eng. J.,* 573-592, December 1974.

Coats, K. H. and Ramesh, A. B., Effects of Grid Type and Difference Scheme on Pattern Steamflood Simulation Results, paper SPE-11079, presented at the 57th Annual Fall Technical Conference and Exhibition of the Society of Petroleum Engineers, New Orleans, La., September 1982.

Colven, W. P., Boone, L. F., Horvath, J. G. and Lorenz, R., Effectiveness of the M-Area Ground Water Remedial Action Program, E. I. DuPont de Nemours and Company, Report DPSP-87-26, Aiken, South Carolina, February 1987.

Eddy, C. A., Looney, B. B., Dougherty, J. M., Hazen, T. C. and Kaback, D. S., Characterization of the Geology, Geochemistry, Hydrology, and Microbiology of the In-Situ Air Stripping Demonstration Site at The Savannah River Site (U), Westinghouse Savannah River Company, Report WSRC-RD-91-21, Aiken, South Carolina, May 1991.

Falta, R. W., Javandel, I., Pruess, K. and Witherspoon, P. A., Density-Driven Flow of Gas in the Unsaturated Zone due to the Evaporation of Volatile Organic Compounds, *Water Resources Research, 25,* (10), 2159-2169, 1989.

Falta, R. W., Pruess, K., Javandel, I. and Witherspoon, P. A., Numerical Modeling of Steam Injection for the Removal of Nonaqueous Phase Liquids from the Subsurface. 1. Numerical Formulation, *Water Resources Research, 28,* (2), 433-449, 1992a.

Falta, R. W., Pruess, K., Javandel, I. and Witherspoon, P. A., Numerical Modeling of Steam Injection for the Removal of Nonaqueous Phase Liquids from the Subsurface. 2. Code Validation and Application, *Water Resources Research, 28,* (2), 451-465, 1992b.

Falta, R. W. and Pruess, K., STMVOC User's Guide, Lawrence Berkeley Laboratory Report LBL-30758, June 1991.

Parker, J. C., Lenhard, R. J. and Kuppusamy, T. A Parametric Model for Constitutive Properties Governing Multiphase Flow in Porous Media, *Water Resources Research, 23,* (4), 618-624, 1987.

Pruess, K., TOUGH User's Guide, Nuclear Regulatory Commission, Report NUREG/CR-4645, June 1987 (also Lawrence Berkeley Laboratory Report LBL-20700, Berkeley, CA., June 1987).

Pruess, K., TOUGH2 - A General-Purpose Numerical Simulator for Multiphase Fluid and Heat Flow, Lawrence Berkeley Laboratory Report LBL-29400, May 1991.

Pruess, K., Grid Orientation and Capillary Pressure Effects in the Simulation of Water Injection into Depleted Vapor Zones, *Geothermics, 20,* (5/6), 257-277, 1991.

Pruess, K. and Bodvarsson, G. S., A Seven-Point Finite Difference Method for Improved Grid Orientation Performance in Pattern Steam Floods, paper SPE-12252, presented at the Seventh Society of Petroleum Engineers Symposium on Reservoir Simulation, San Francisco, 1983.

Stone, H. L., Probability Model for Estimating Three-Phase Relative Permeability, *Trans. SPE of AIME, 249,* 214-218, 1972.

Todd, M. R., O'Dell, P. M. and Hirasaki, G. J., Methods for Increased Accuracy in Numerical Reservoir Simulators, *Soc. Pet. Eng. J.,* 515-530, December 1972.

Tsang, Y. W. and Pruess, K., Preliminary Studies of Gas Phase Flow Effects and Moisture Migration at Yucca Mountain, Lawrence Berkeley Laboratory Report LBL-28819, Berkeley, CA, 1989.

Yanosik, J. L. and McCracken, T. A., A Nine-Point, Finite Difference Reservoir Simulator for Realistic Prediction of Adverse Mobility Ratio Displacements, *Soc. Pet. Eng. J.,* 253-262, August 1979.

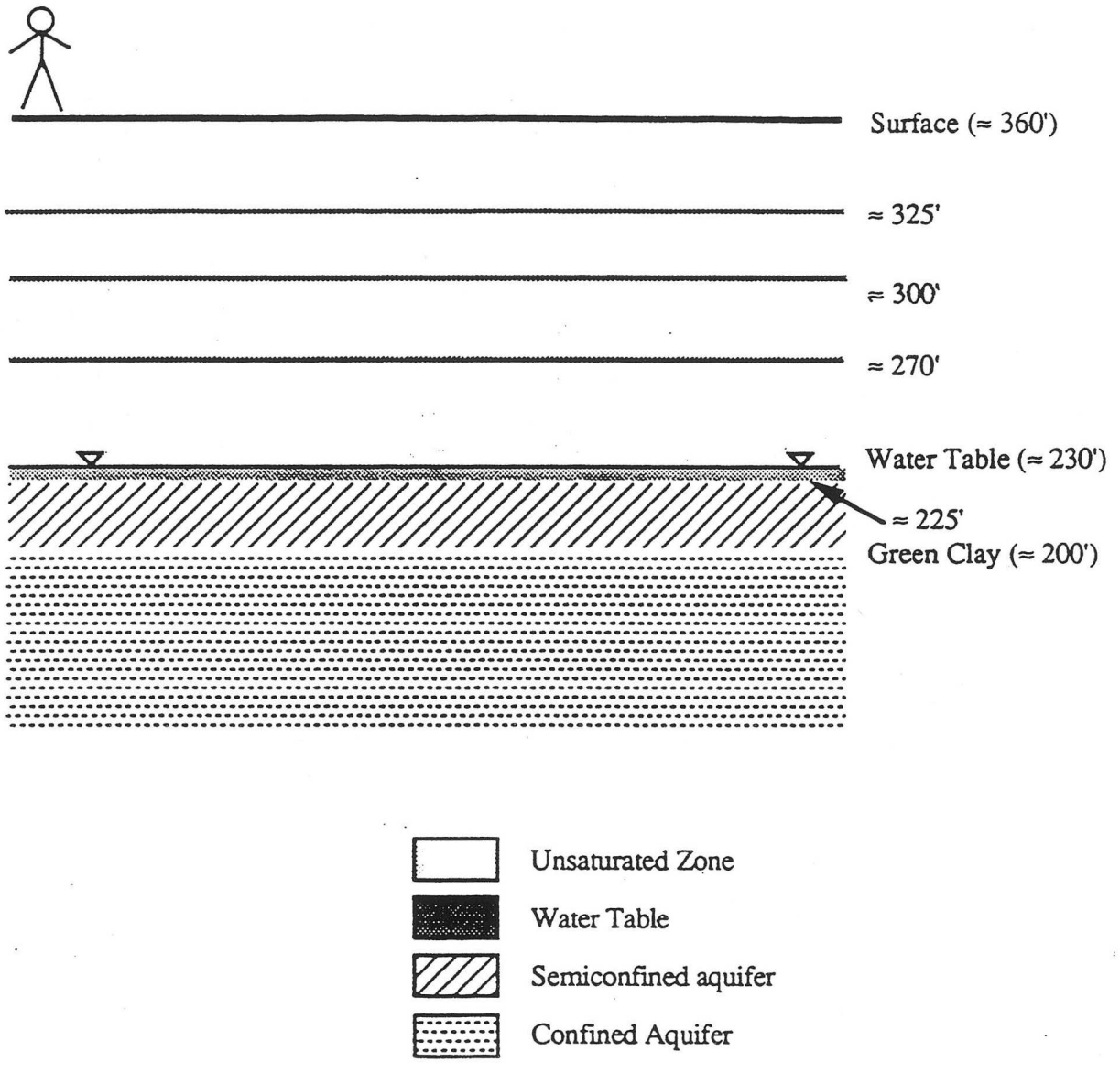

Figure 1. Schematic diagram of hydrogeologic features at the site of the Savannah River Integrated Demonstration Project (from Eddy et al., 1991).

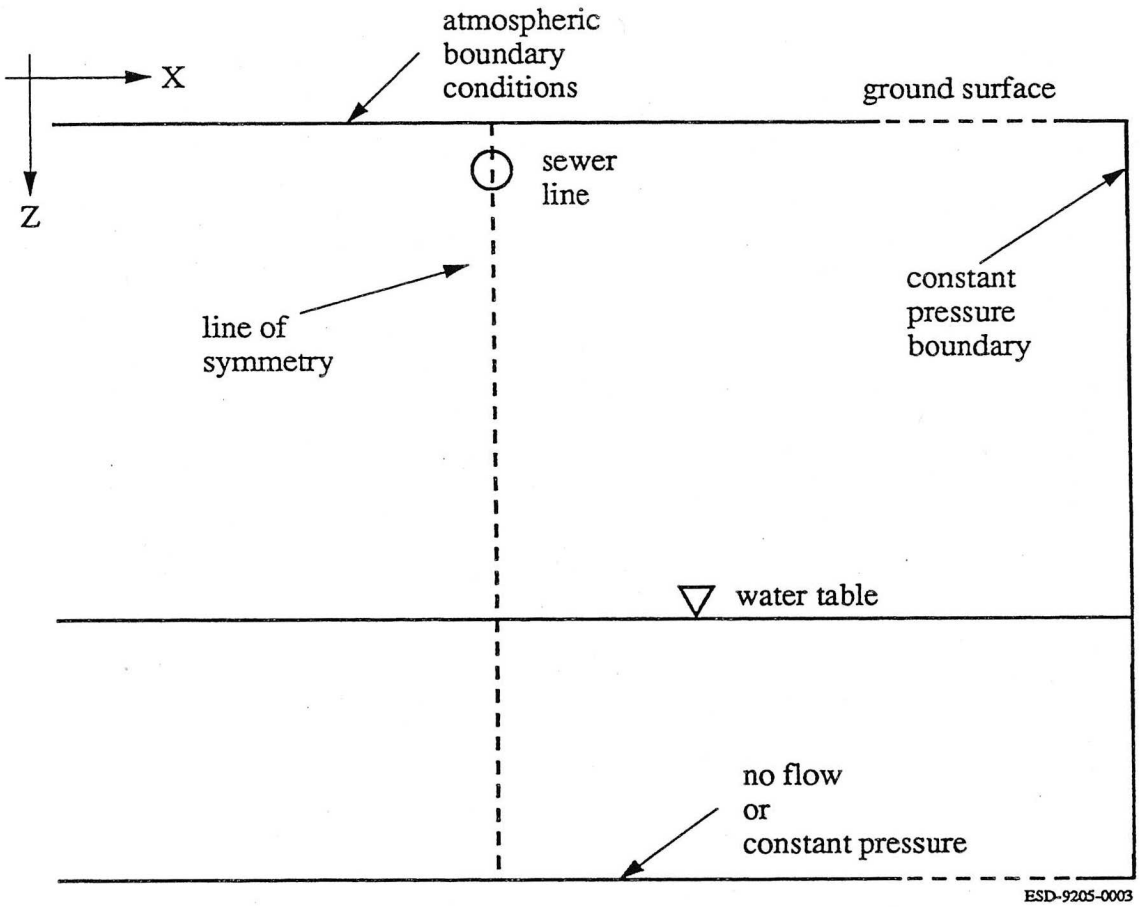

Figure 2. Schematic of model system.

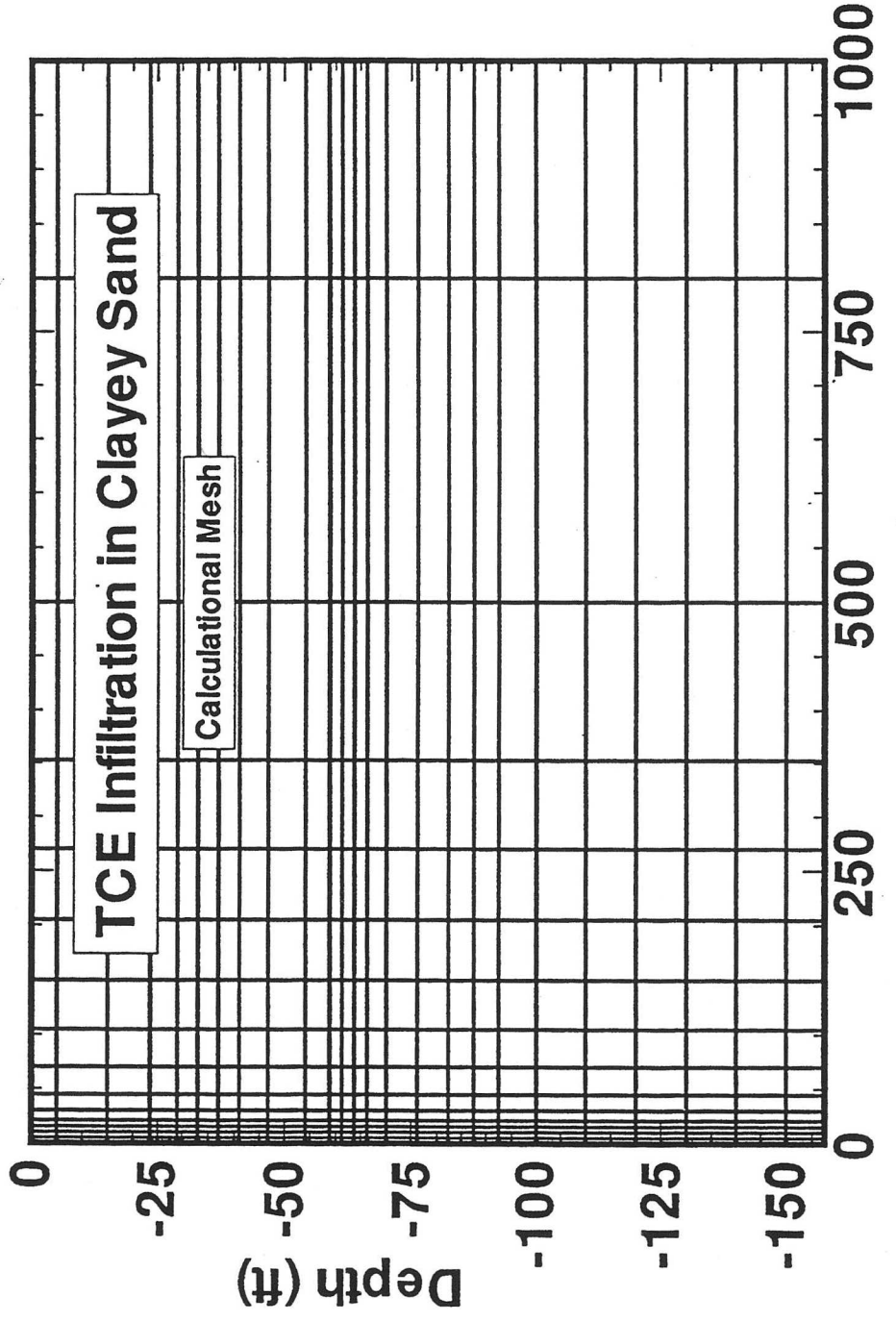

Figure 3. Vertical section numerical grid used in the simulations.

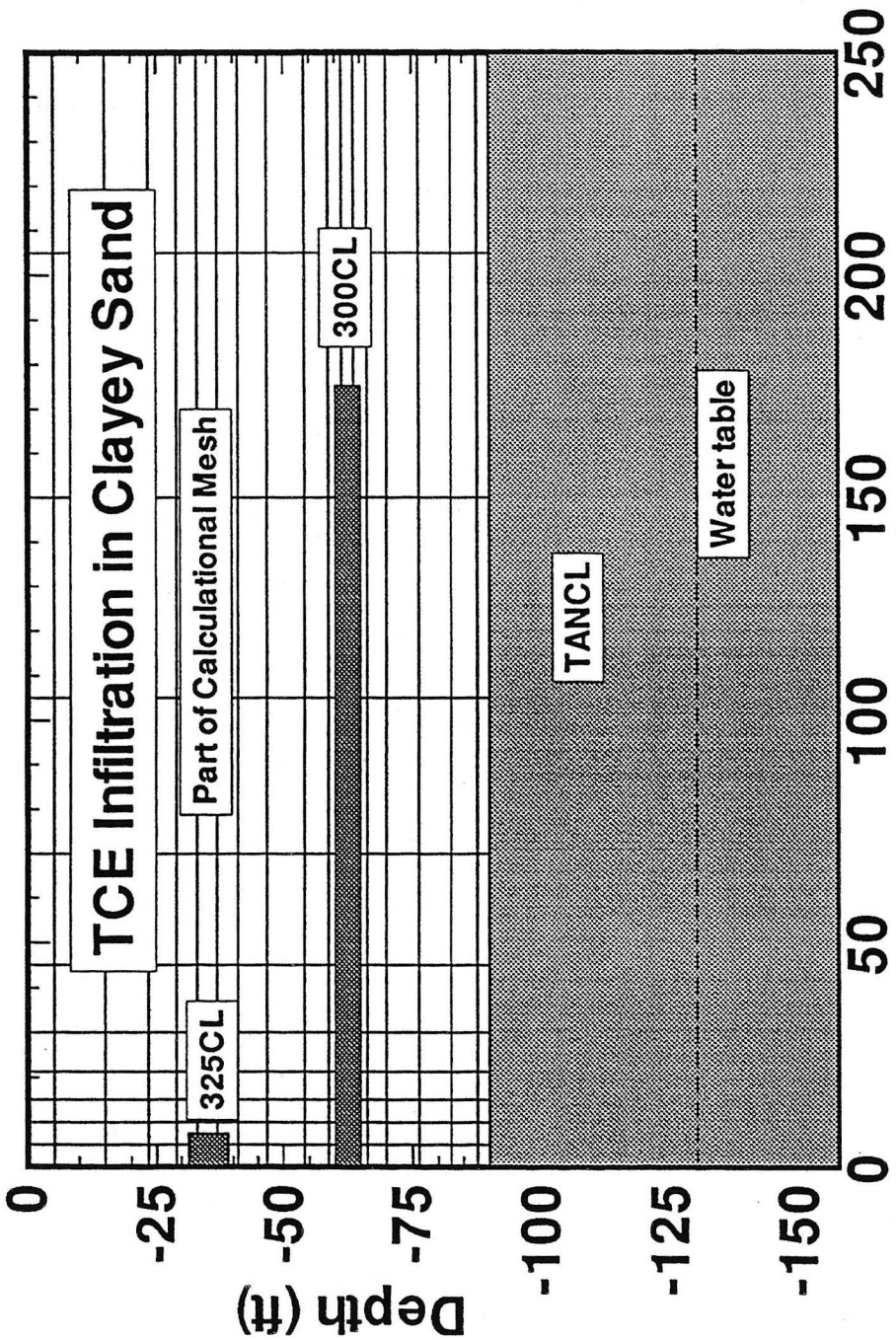

Figure 4. Numerical grid with low-permeability clay zones.

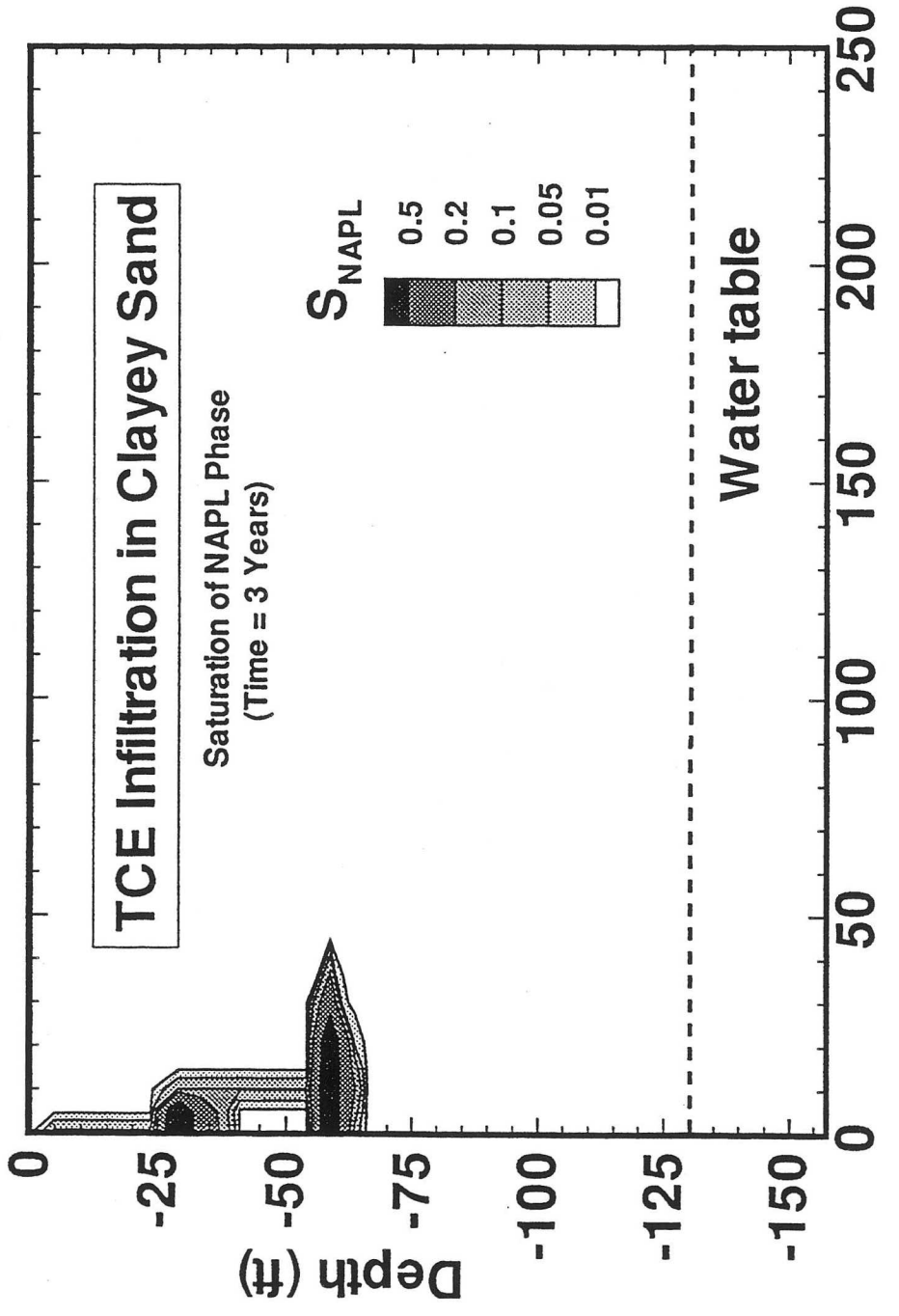

Figure 5. Saturation of NAPL phase after 3 years of infiltration.

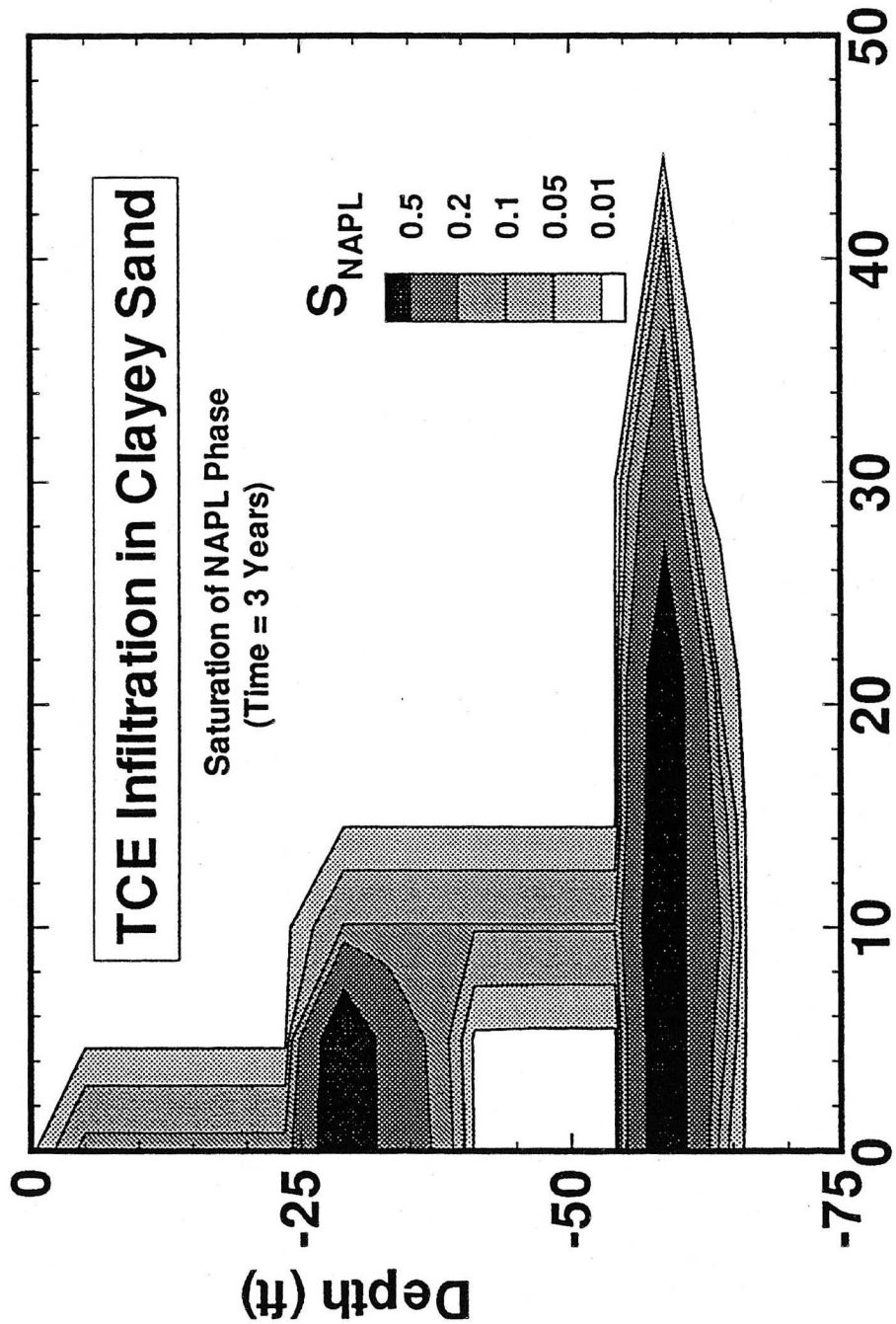

Figure 6. NAPL saturation after 3 years of infiltration (detail).

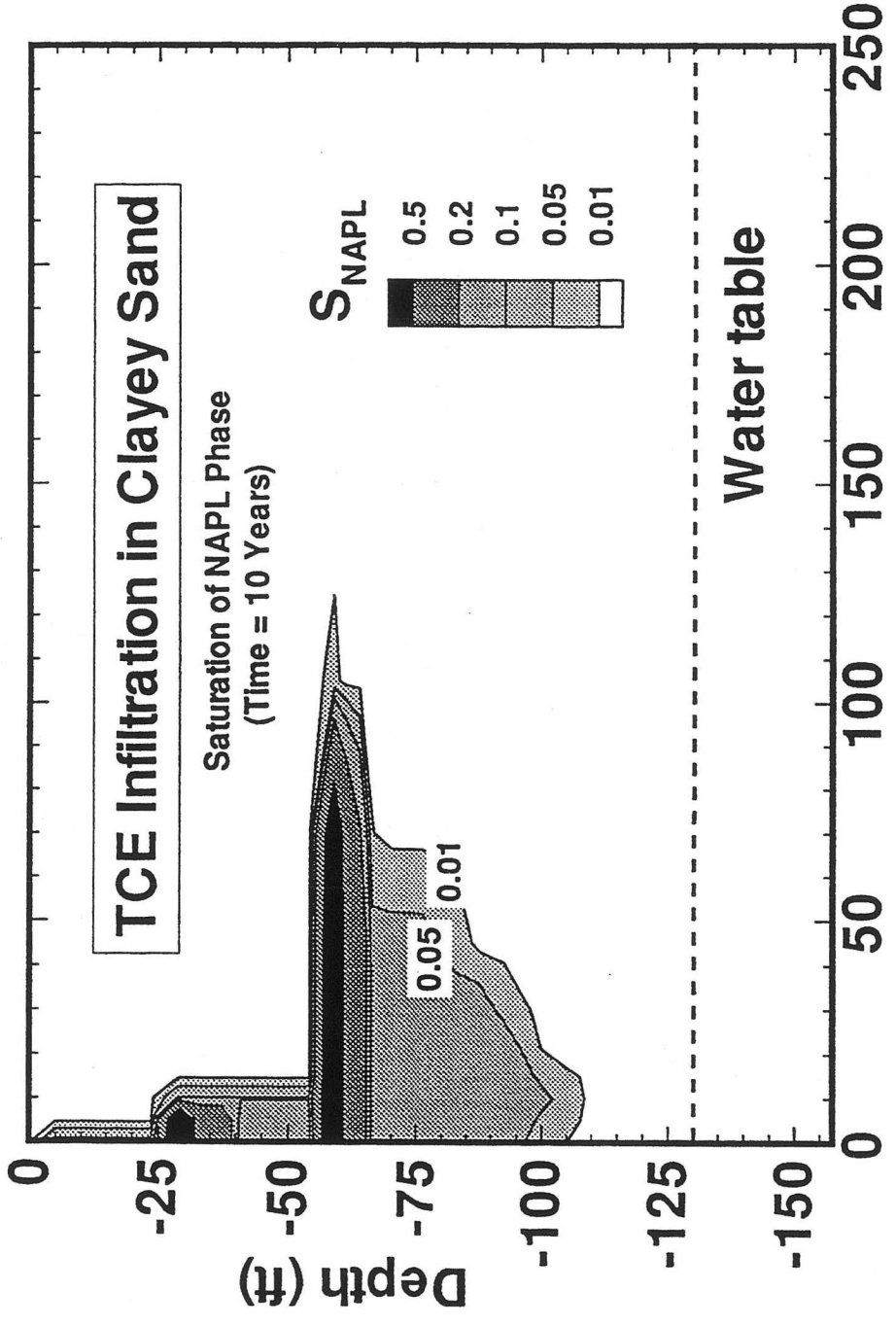

Figure 7. NAPL saturation after 10 years of infiltration.

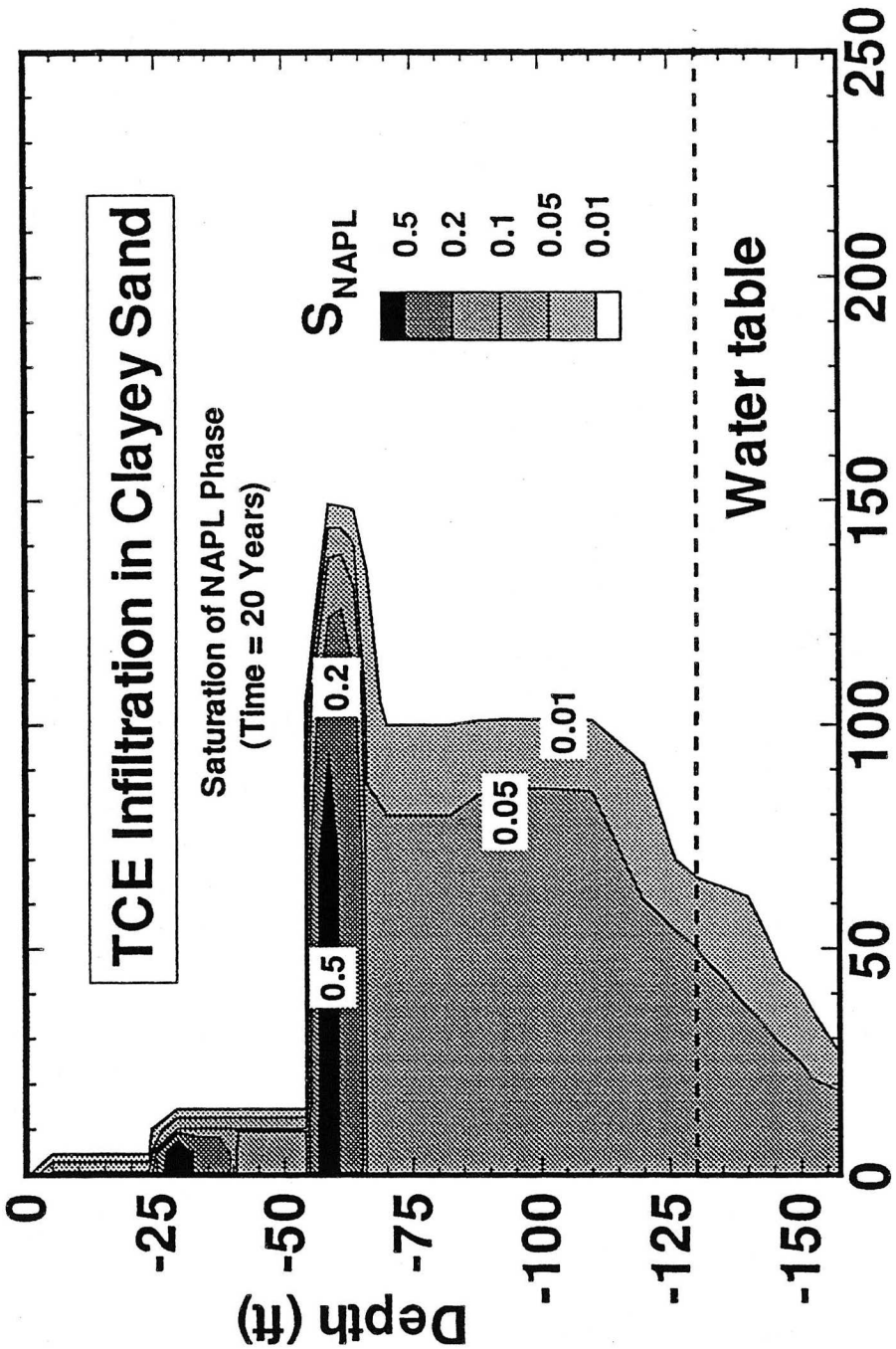

Figure 8. NAPL saturation after 20 years of infiltration.

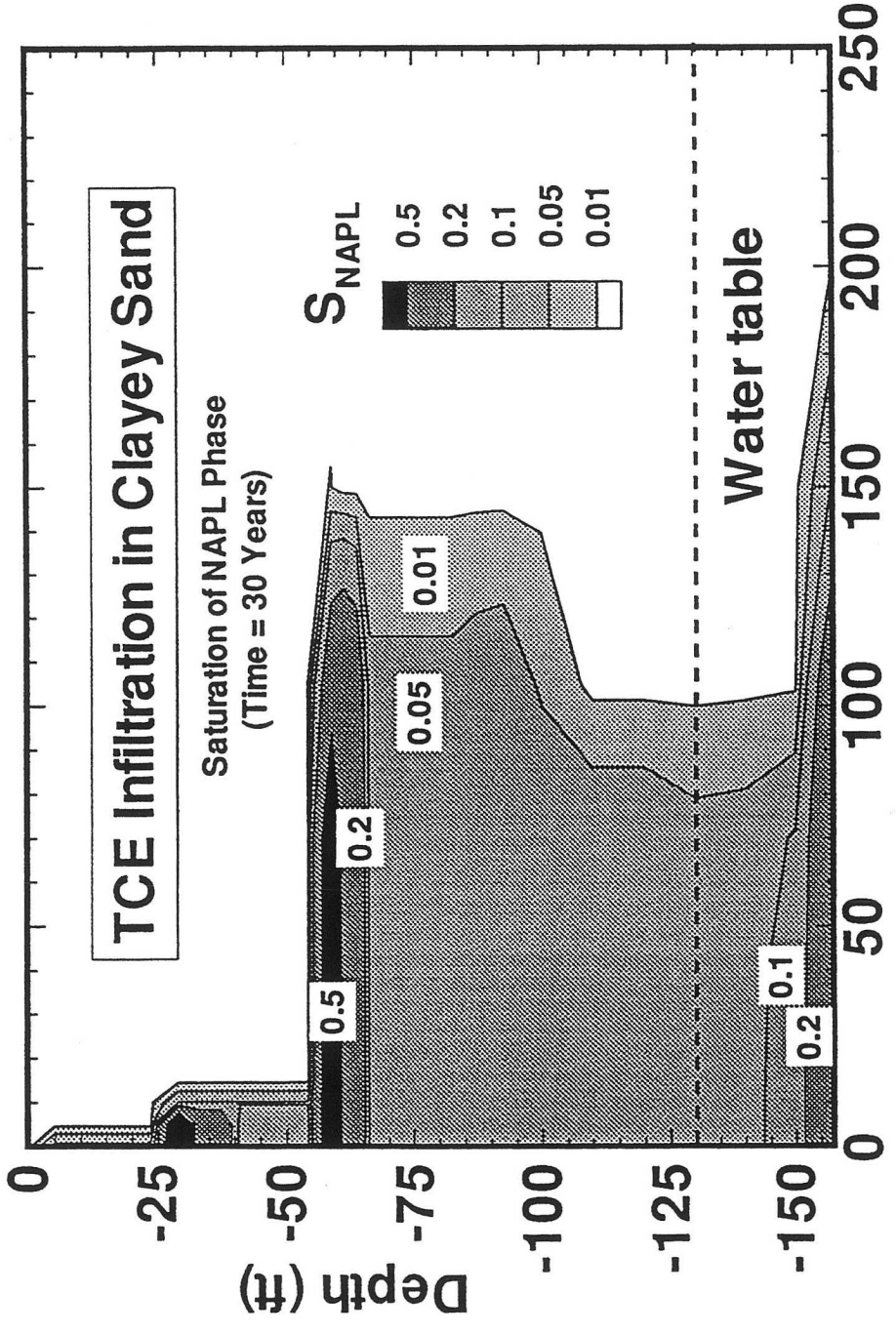

Figure 9. NAPL saturation after 30 years of infiltration.

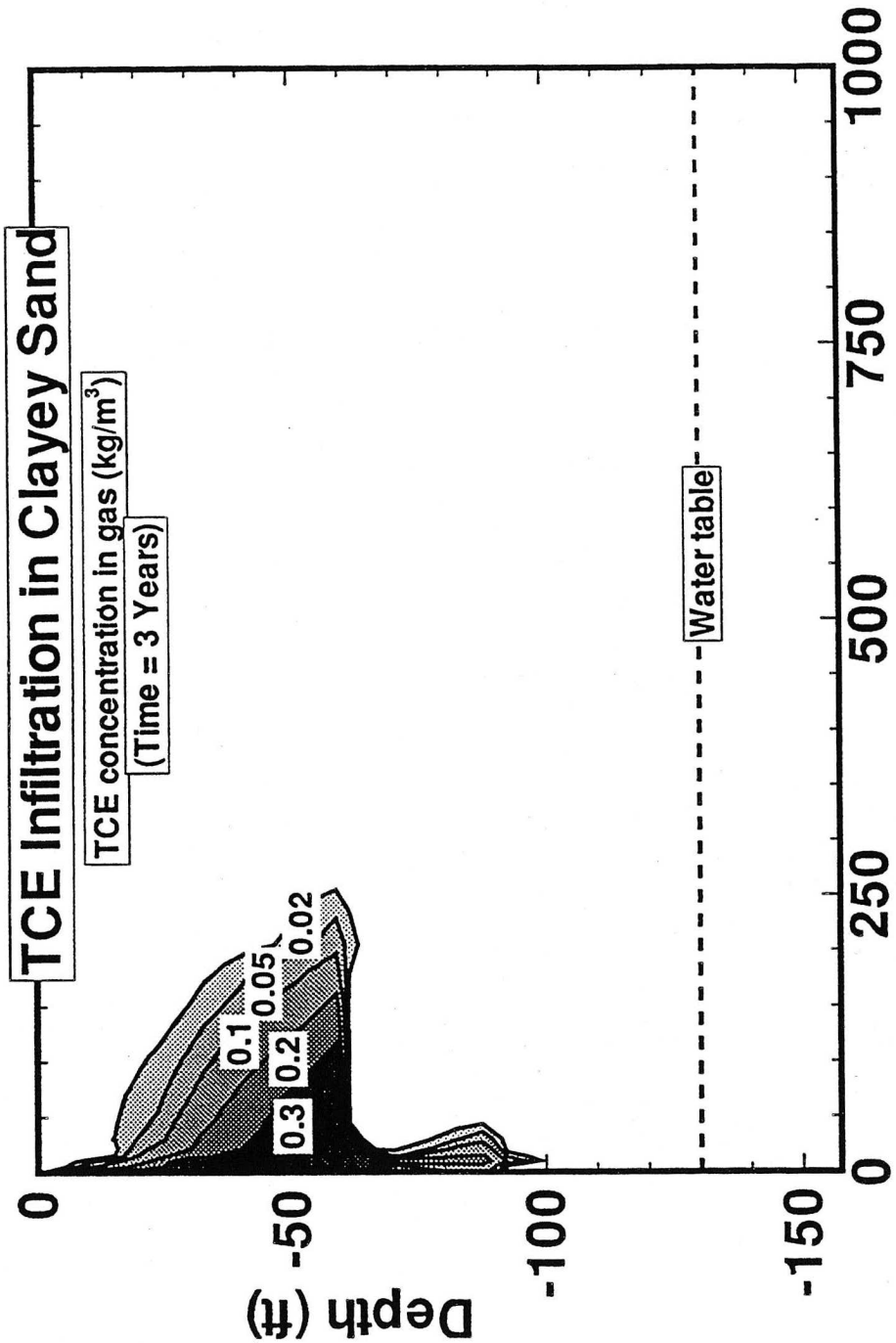

Figure 10. Concentration of TCE in the gas phase, after 3 years of infiltration.

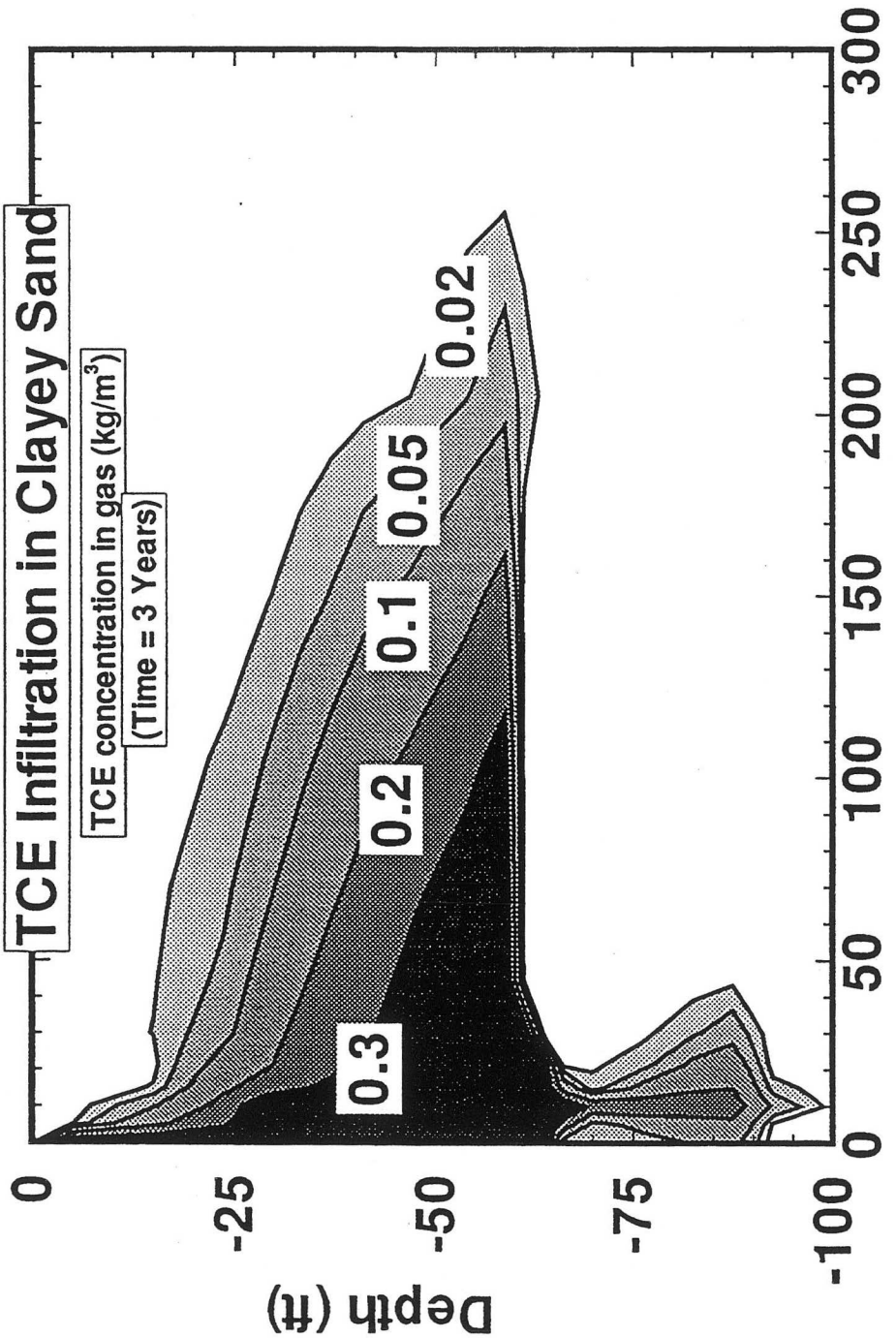

Figure 11. Concentration of TCE in the gas phase, after 3 years of infiltration (detail).

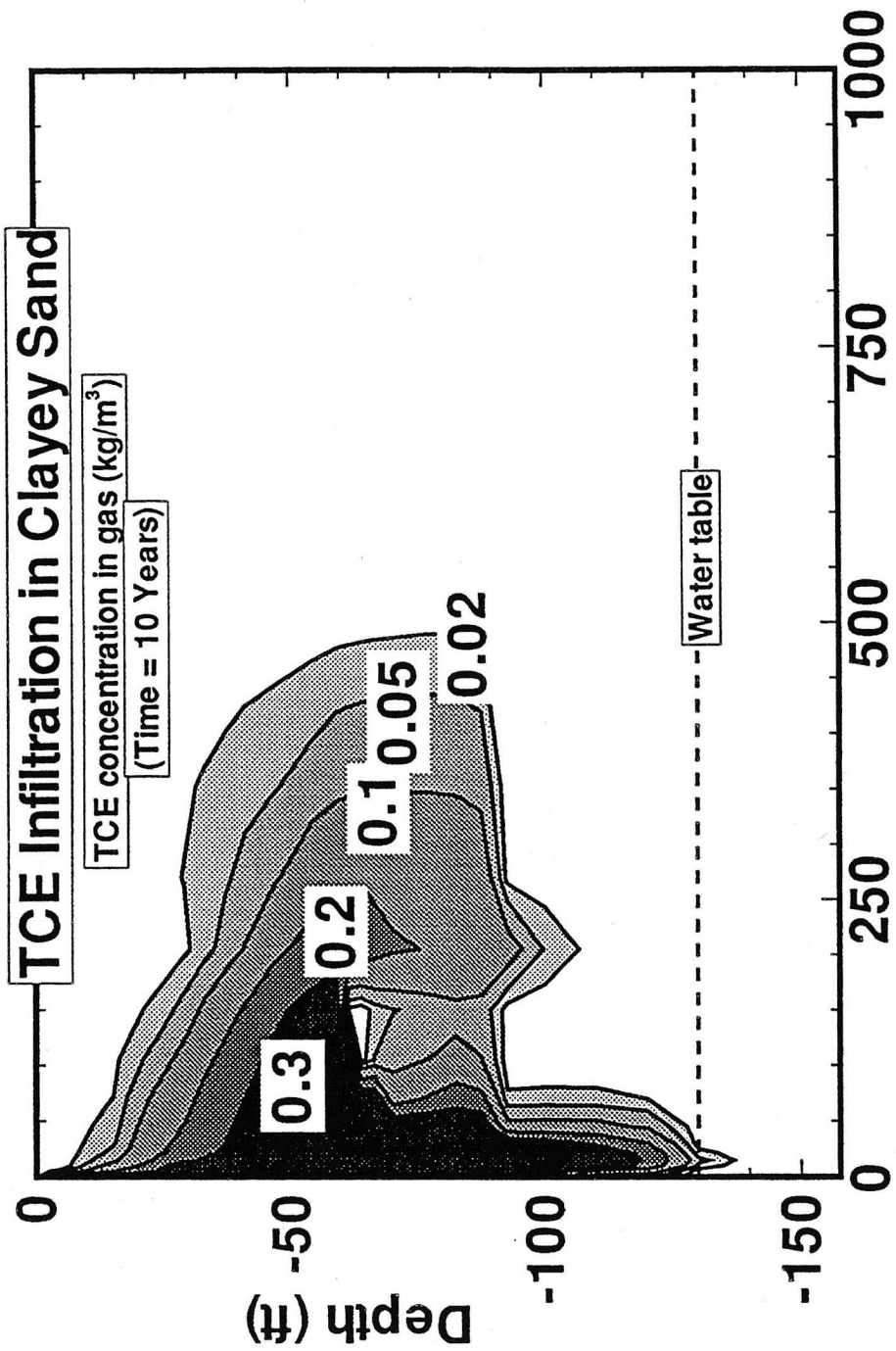

Figure 12. Concentration of TCE in the gas phase, after 10 years of infiltration.

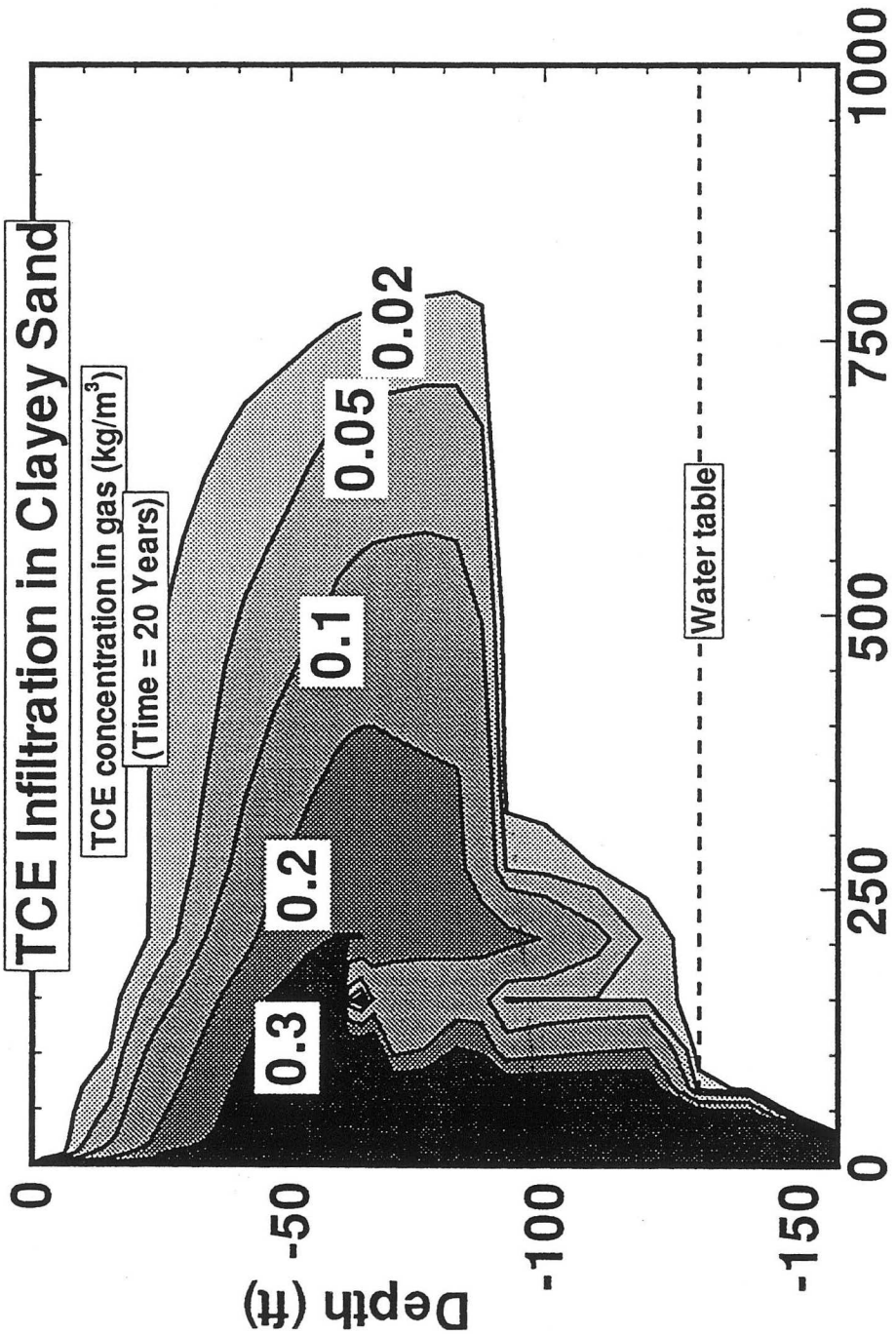

Figure 13. Concentration of TCE in the gas phase, after 20 years of infiltration.

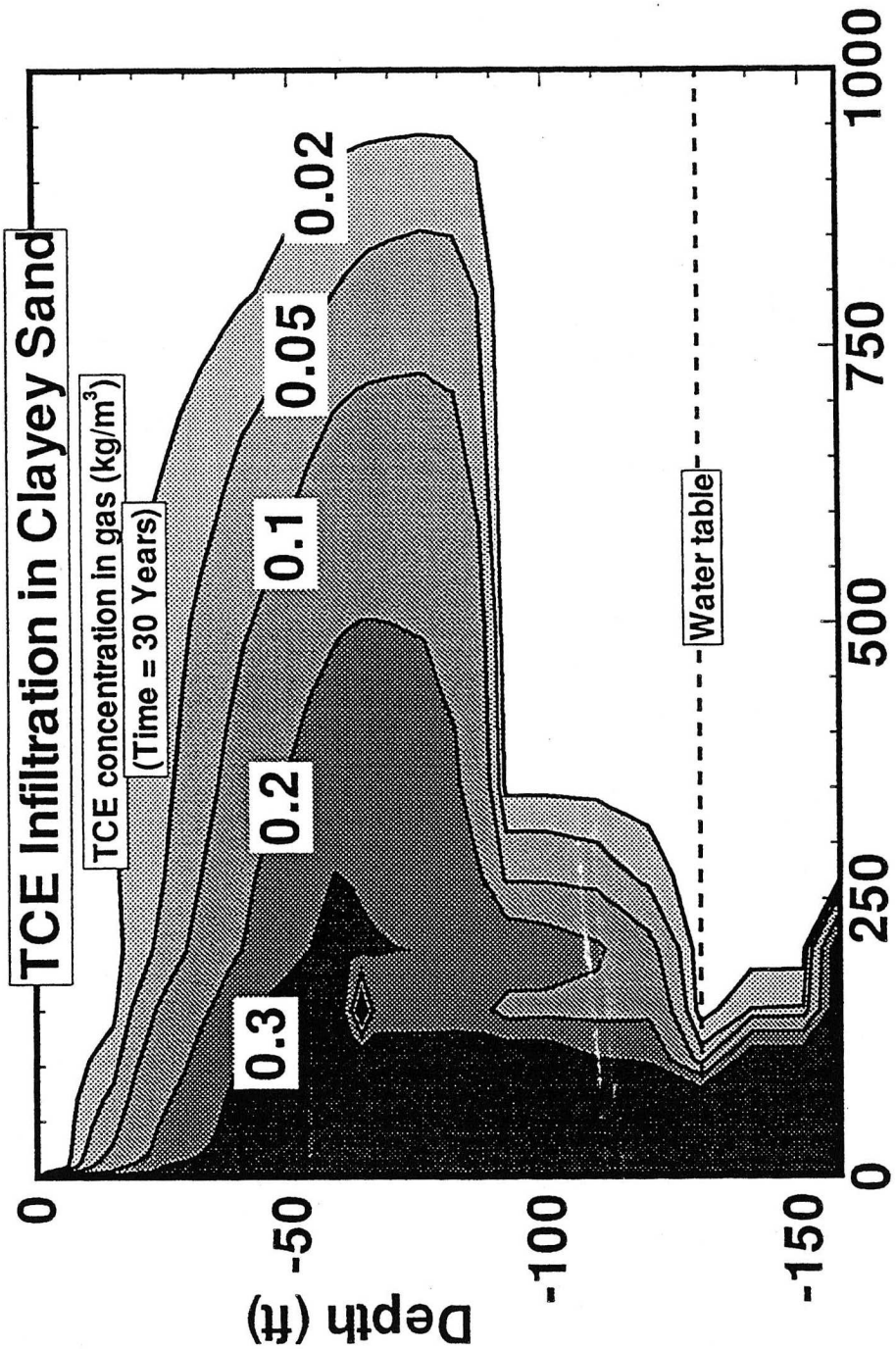

Figure 14. Concentration of TCE in the gas phase, after 30 years of infiltration.

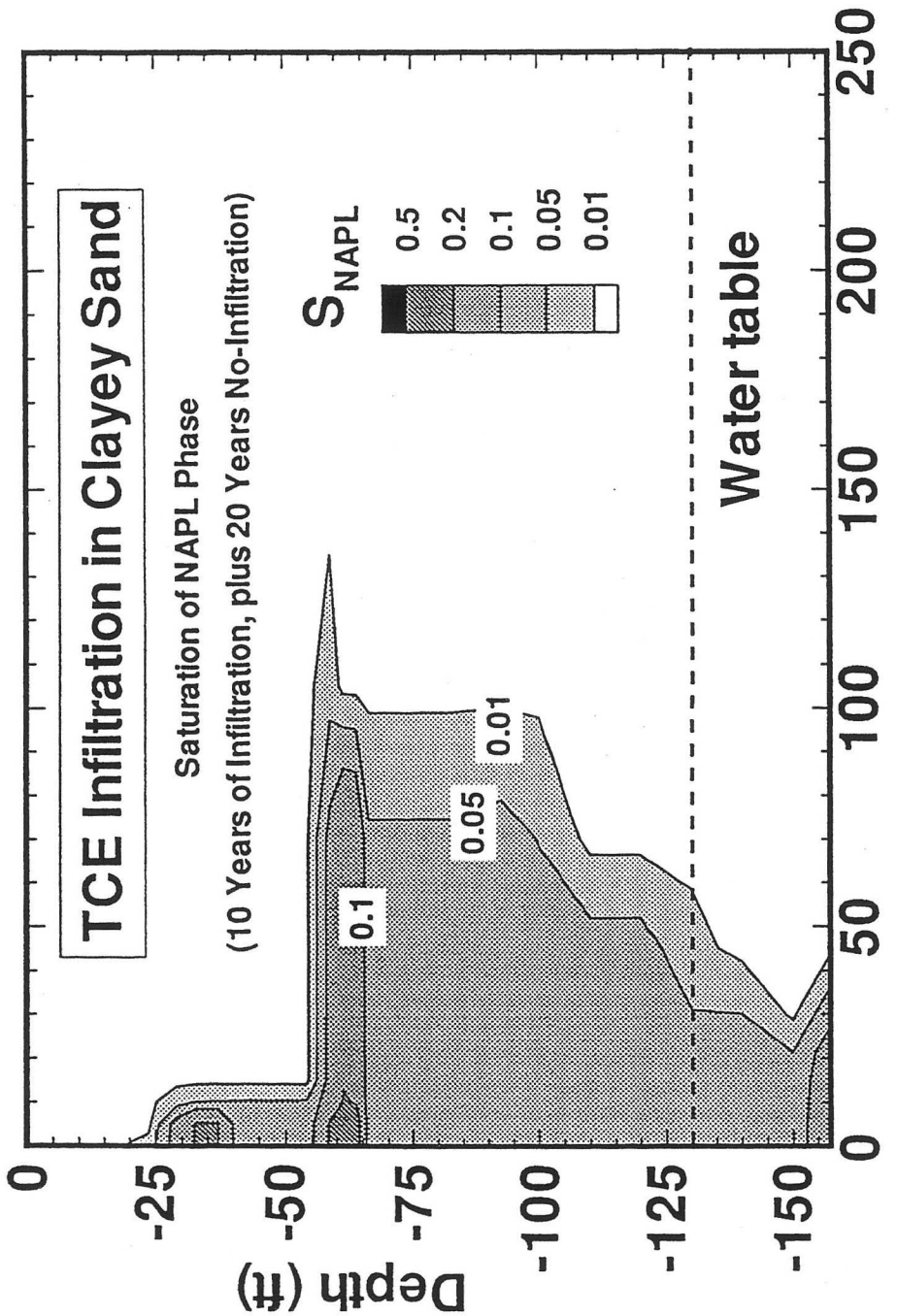

Figure 15. NAPL saturation after 10 years of infiltration, followed by 20 years without infiltration.

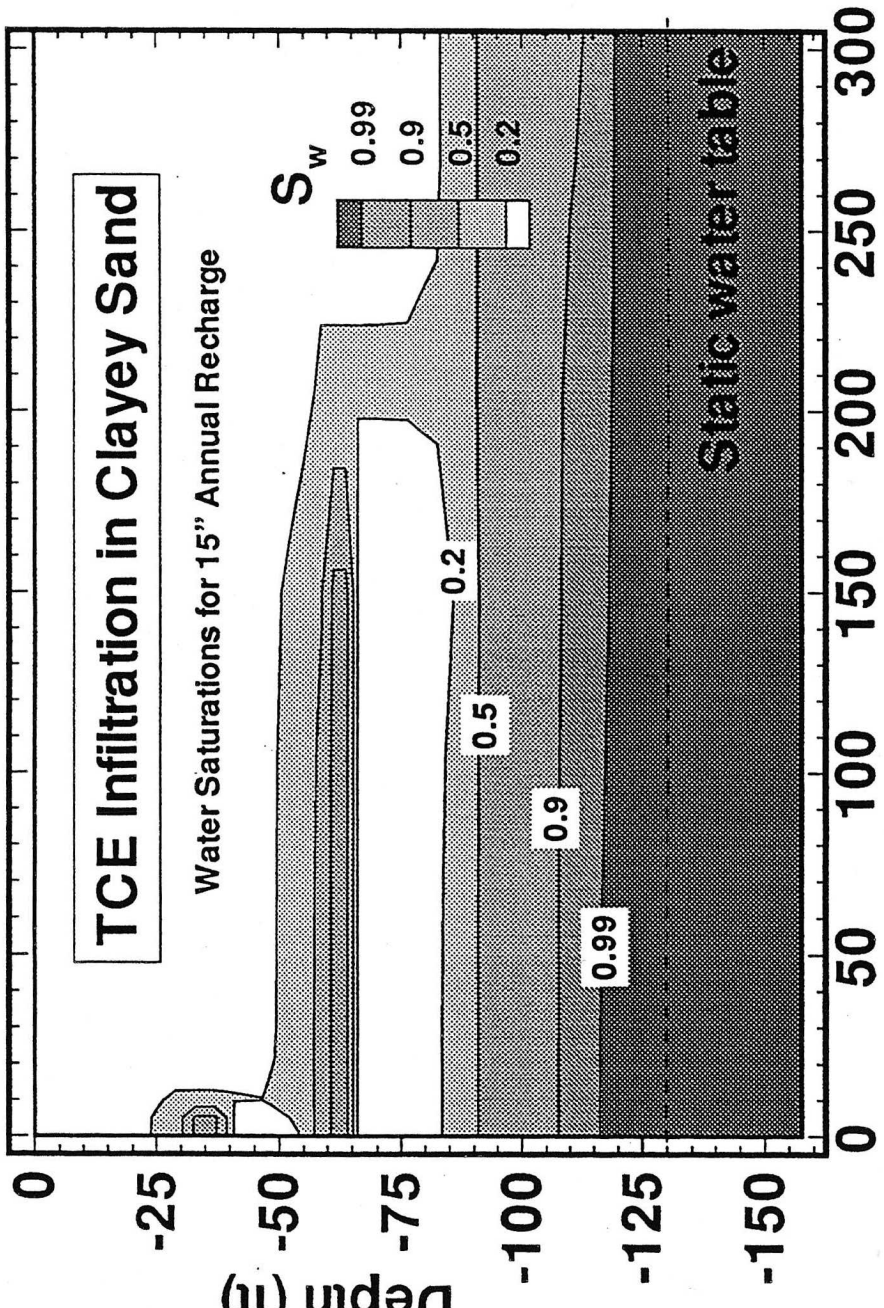

Figure 16. Steady-state water saturations under conditions of 15 inch annual recharge.

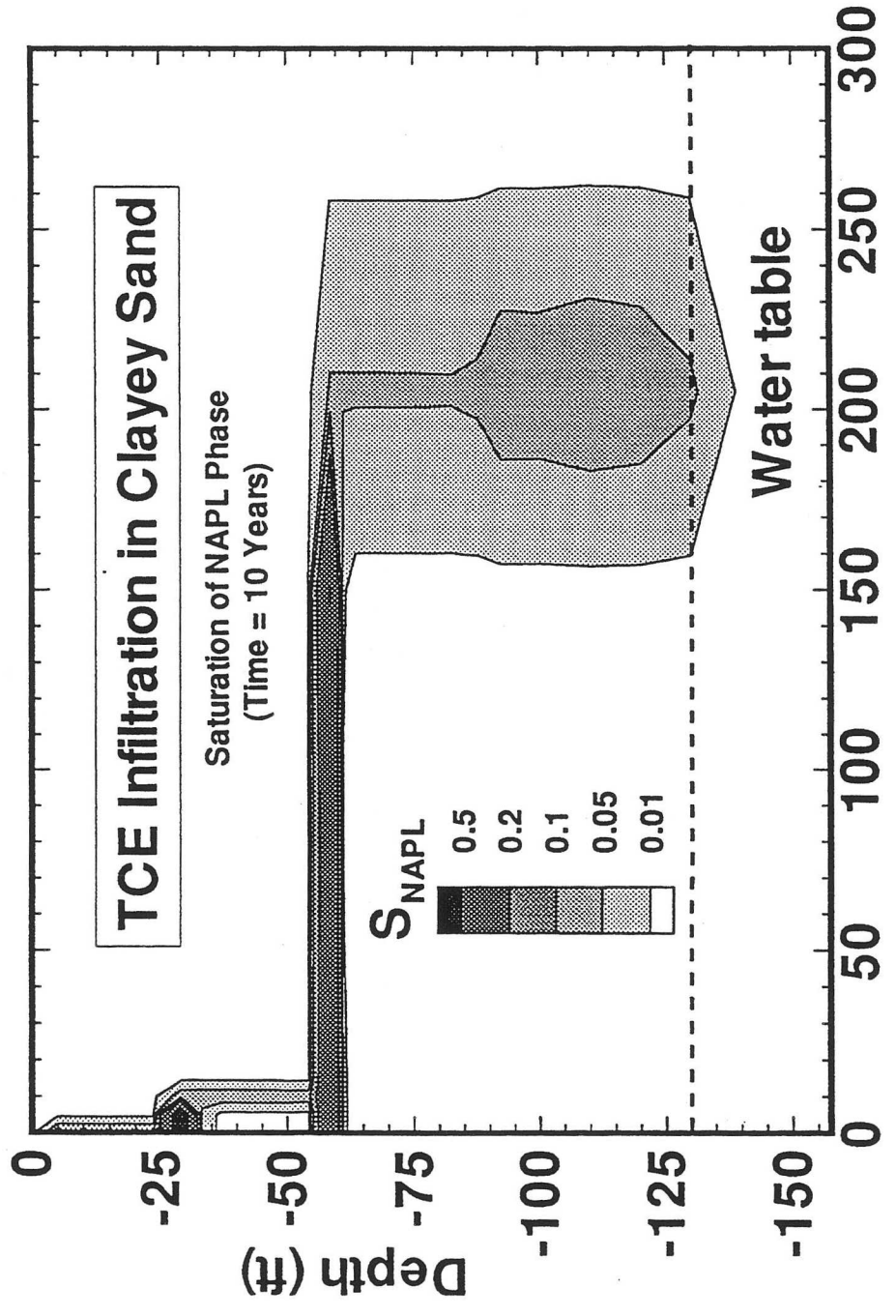

Figure 17. NAPL saturation after 10 years of infiltration, in system with 15 inch annual recharge.

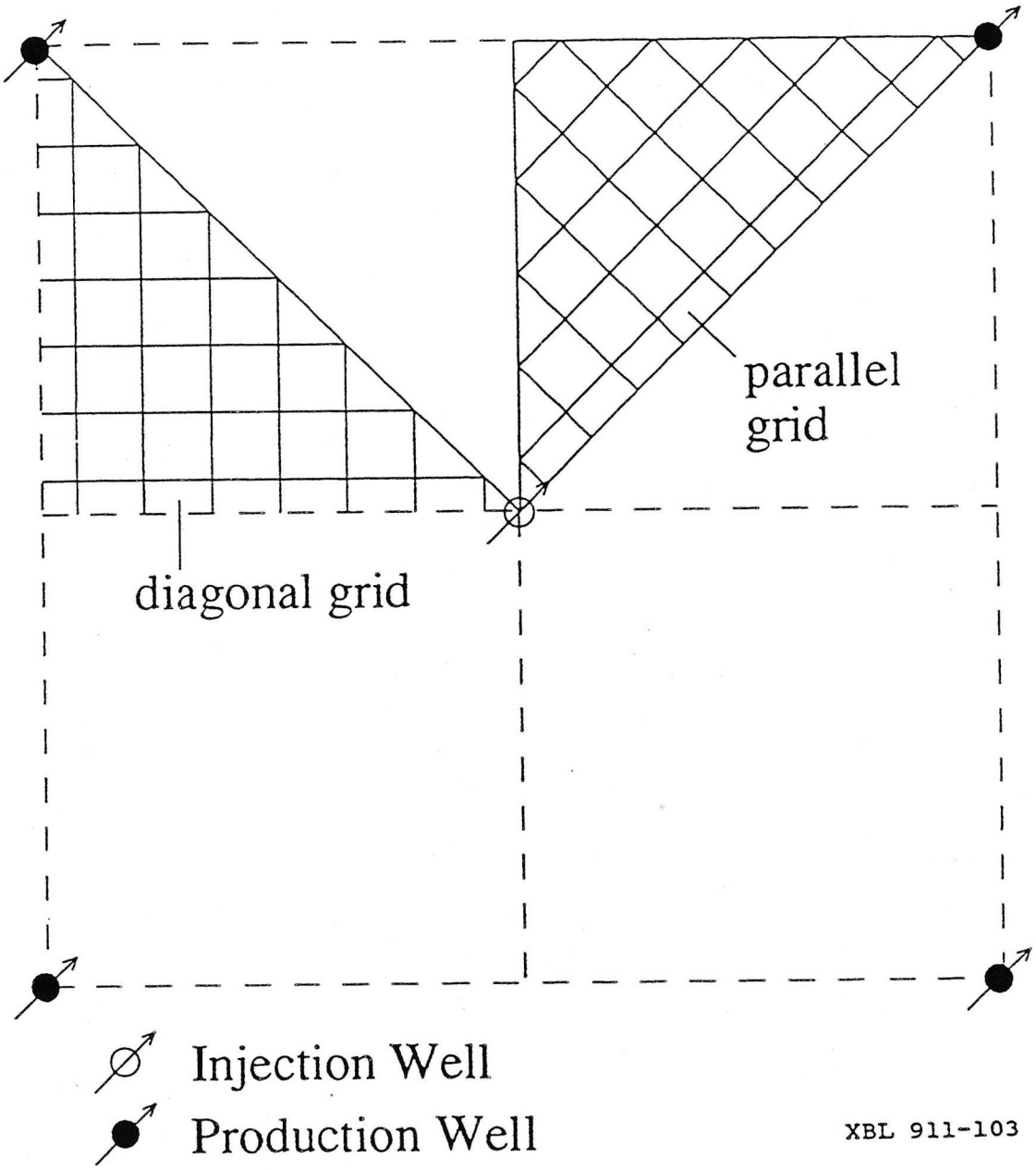

Figure 18. Five-spot well pattern with parallel and diagonal grids for modeling a 1/8 symmetry domain.

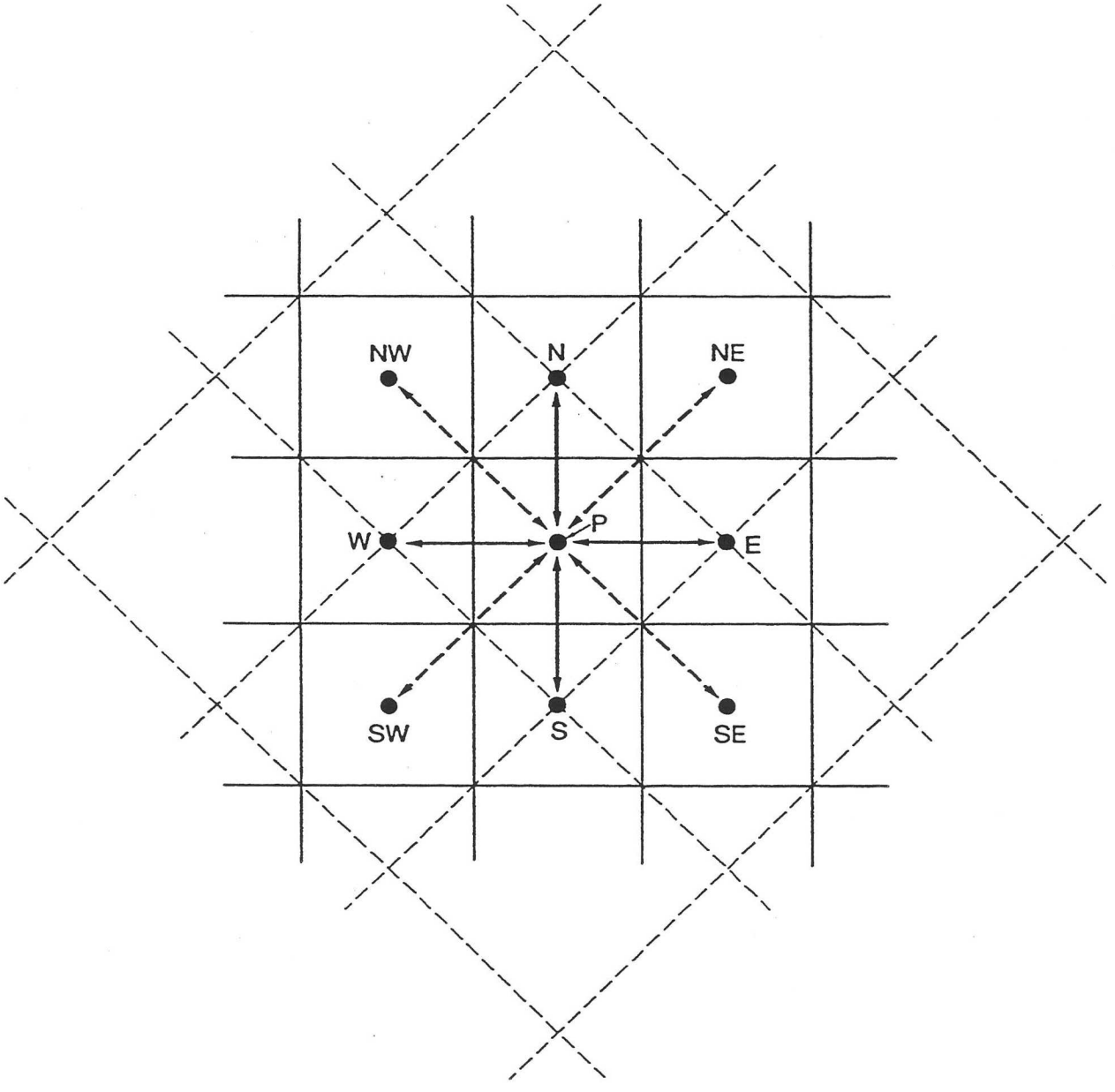

Figure 19. Five- and nine-point finite difference approximations (modified from Pruess and Bodvarsson, 1983).

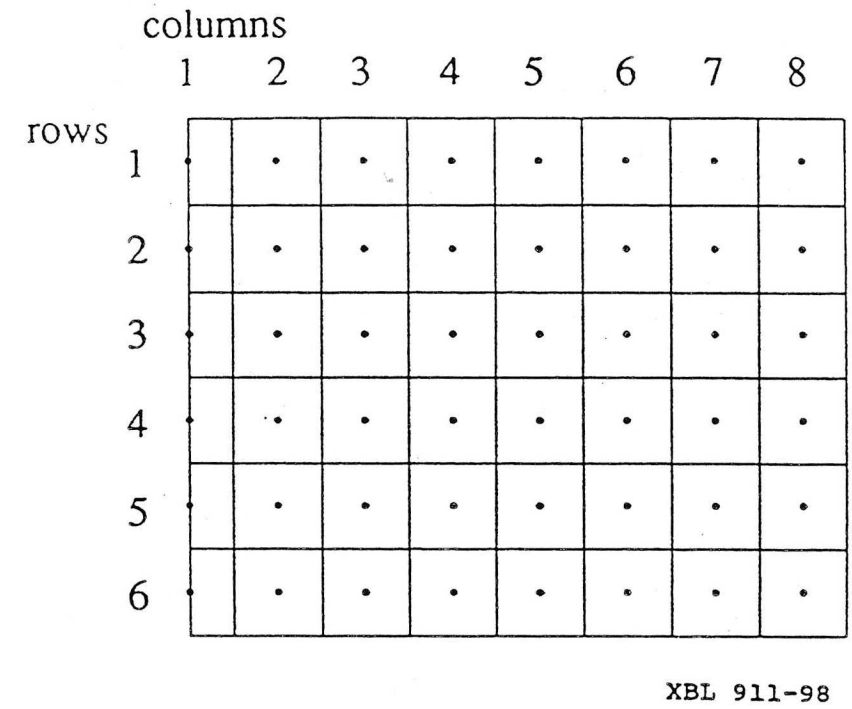

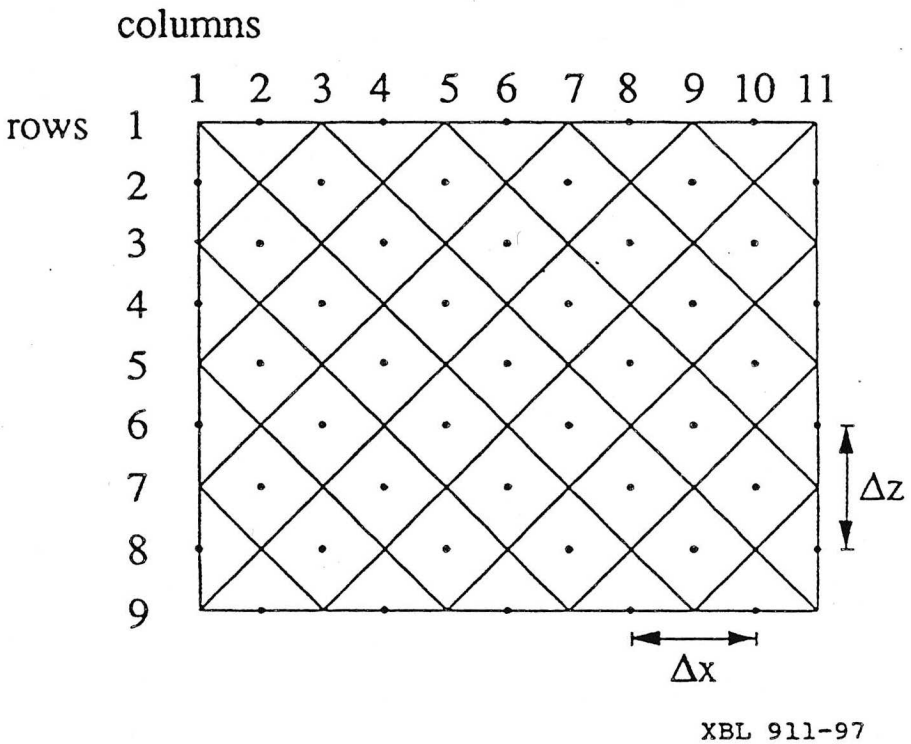

Figure 20. Schematic of parallel and diagonal grids used for modeling injection in 2-D vertical sections (from Pruess, 1991).

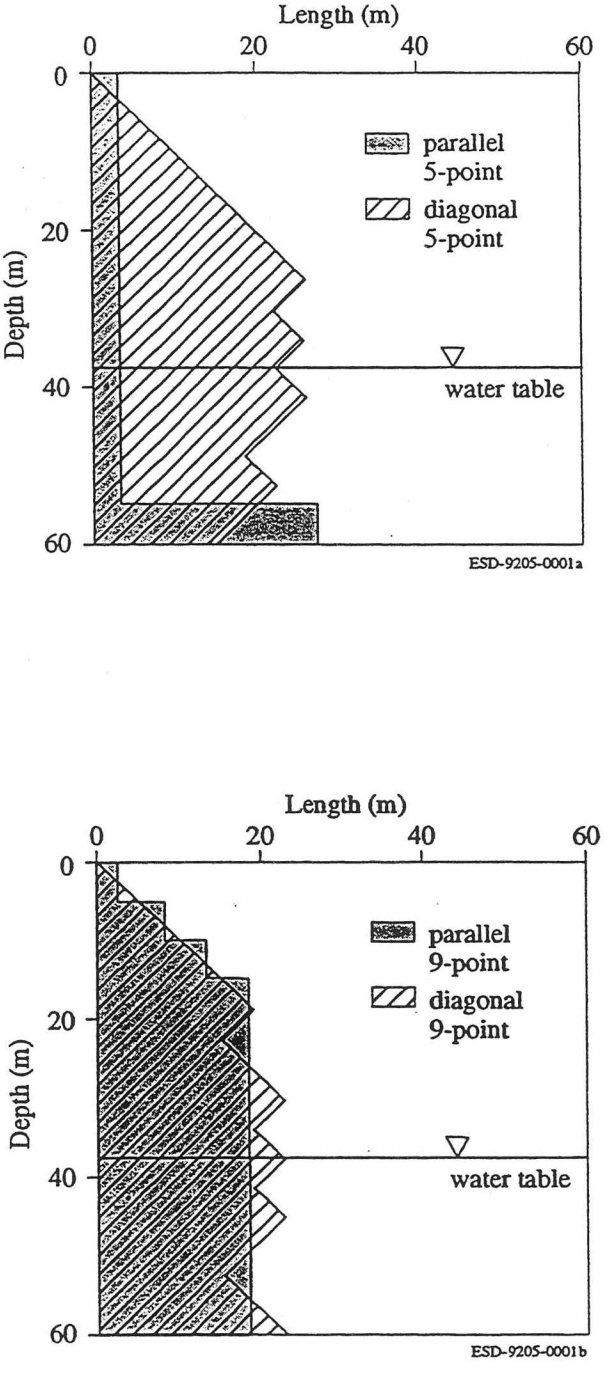

Figure 21. TCE plumes after 10 years of infiltration, using parallel and diagonal vertical section grids with 5- and 9-point finite difference approximations.

LAWRENCE BERKELEY LABORATORY
UNIVERSITY OF CALIFORNIA
TECHNICAL INFORMATION DEPARTMENT
BERKELEY, CALIFORNIA 94720